AD-A052 749 ARMY MISSILE RESEARCH AND DEVELOPMENT COMMAND REDSTO--ETC F/G 18/6
AN EXPERIMENTAL TECHNIQUE TO EVALUATE THE BLOW-OFF EFFECTS OF N--ETC(U)
SEP 77 J A SCHAEFFEL, B R MULLINIX

UNCLASSIFIED DRDMI-TL-77-10 NL

| OF |

AD
A052749

END
DATE
FILMED
5-78
DDC

U.S. ARMY
MISSILE
RESEARCH
AND
DEVELOPMENT
COMMAND

Redstone Arsenal, Alabama 35809

TECHNICAL REPORT TL-77-10

AN EXPERIMENTAL TECHNIQUE TO EVALUATE THE BLOW-OFF EFFECTS OF NUCLEAR WEAPONS

John A. Schaeffel and Bobby R. Mullinix
Ground Equipment and Missile Structures Directorate
Technology Laboratory

William F. Ranson
Auburn University

16 September 1977

APPROVED FOR PUBLIC RELEASE; DISTRIBUTION UNLIMITED.

DMI FORM 1000, 1 APR 77

DISPOSITION INSTRUCTIONS

DISCLAIMER

TRADE NAMES

SECURITY CLASSIFICATION OF THIS PAGE (When Data Entered)

REPORT DOCUMENTATION PAGE

READ INSTRUCTIONS BEFORE COMPLETING FORM

1. REPORT NUMBER
TL-77-10 14 DRDMI-TL-77-10

2. GOVT ACCESSION NO.

3. RECIPIENT'S CATALOG NUMBER

4. TITLE (and Subtitle)
6 AN EXPERIMENTAL TECHNIQUE TO EVALUATE THE BLOW-OFF EFFECTS OF NUCLEAR WEAPONS.

5. TYPE OF REPORT & PERIOD COVERED
9 Technical Rep[redacted]t.

6. PERFORMING ORG. REPORT NUMBER
TL-77-10

7. AUTHOR(s)
10 John A./Schaeffel [redacted] Bobby R./Mullinix
William F./Ranson ~~Auburn University~~

8. CONTRACT OR GRANT NUMBER(s)
12 62p.

9. PERFORMING ORGANIZATION NAME AND ADDRESS
Commander
US Army Missile Research and Development Command
Attn: DRDMI-TL
Redstone Arsenal, Alabama 35809

10. PROGRAM ELEMENT, PROJECT, TASK AREA & WORK UNIT NUMBERS
16 DA 1L362303A214
~~AMCMS 632303.112140811.01~~

11. CONTROLLING OFFICE NAME AND ADDRESS
Commander
US Army Missile Research and Development Command
Attn: DRDMI-TI
Redstone Arsenal, Alabama 35809

12. REPORT DATE
11 16 Sep[redacted]77

13. NUMBER OF PAGES
59

14. MONITORING AGENCY NAME & ADDRESS (if different from Controlling Office)

15. SECURITY CLASS. (of this report)
UNCLASSIFIED

15a. DECLASSIFICATION/DOWNGRADING SCHEDULE

16. DISTRIBUTION STATEMENT (of this Report)

Approved for public release; distribution unlimited.

17. DISTRIBUTION STATEMENT (of the abstract entered in Block 20, if different from Report)

18. SUPPLEMENTARY NOTES

19. KEY WORDS (Continue on reverse side if necessary and identify by block number)

Nuclear weapons effects	Blow-off
Missile structures	Optical techniques
X-ray effects	High speed photography

20. ABSTRACT (Continue on reverse side if necessary and identify by block number)

An experimental technique to simulate and evaluate the effects of high concentrations of x-rays resulting from a nuclear detonation on missile structures is presented. Data from 34 tests are included to demonstrate the technique. The effects of variations in the foil thickness, capacitor voltage, and plate thickness on the total impulse and maximum strain in the structure were determined. The experimental technique utilizes a high → next page

ABSTRACT (Continued)

DD FORM 1 JAN 73 1473 EDITION OF 1 NOV 65 IS OBSOLETE

UNCLASSIFIED
SECURITY CLASSIFICATION OF THIS PAGE (When Data Entered)

410 263 #ll

ABSTRACT (Continued)

energy capacitor discharge unit to explode an aluminum foil on the surface of the structure. The structural response is evaluated by optical methods using the grid slope deflection method. The fringe patterns were recorded using a high-speed framing camera. The data were digitized using an optical comparator with an x-y table. The analysis was performed on a CDC 6600 computer.

CONTENTS

ACKNOWLEDGMENTS

The authors express their gratitude and deep appreciation to Mr. V. G. Irelan for his assistance with the control system electronics and to Mr. W. B. Matkin and Ms. D. K. Russell for their aid with the laboratory work and data reduction.

I. INTRODUCTION

The three broad divisions of nuclear weapons effects are blast, thermal radiation, and nuclear radiation. Blast effects include air-blast, cratering, and ground shock. Thermal radiation includes the effects of heat and light. The divisions of nuclear radiation are (a) the initial effects which include gamma and neutron radiation and (b) the residual effects which include induced radiation and fallout. The alpha and beta effects are significant only within distances of approximately 2 meters of ground zero and are therefore negligible in comparison with other effects.

Restrictions placed on nuclear testing by regulations, treaties, and costs made it imperative that a large portion of the nuclear weapons effects research be done through experimental and simulation techniques.

The objective of this research is to develop an experimental technique to simulate and evaluate the effects of high concentrations of x-rays resulting from a nuclear detonation on missile structures (blow-off) and perform basic tests to establish the validity of the technique.

Prior research investigated the effects of nuclear weapons on missile structures while subjected to the combined loading conditions encountered in a flight environment [1]. The primary effects considered were pre-stress due to flight loads, pressure from the air blast, and heat from the flight environment plus thermal radiation from the detonation.

The two energy sources considered to explode the foil on the surface were a high energy capacitor discharge unit and a laser. The high energy capacitor discharge unit was selected.

Several existing methods measure the slope of deformed plates using grids projected on the reflecting surface of flat plates [2,3,4]. However, these methods are usually considered cumbersome and more immediate Moire' techniques have been developed which record partial slopes directly. The first was a double exposure method developed by Ligtenberg [5]. In this method, Ligtenberg photographed a grating reflected off the surface of a polished plate before deformation. After deformation a second exposure was made of the grating projected on the plate. The result is a Moire' pattern appearing on the negative that shows the partial slope contours of the plate in the principal directions of the grid lines. Rieder and Ritter [6] improved the accuracy of this method by using a partial mirror and a line grating of a greater density. Finally, Chiang [7] has used the method of Rieder and Ritter to measure the partial slopes of plates subjected to a dynamic loading. A complete description of the different techniques and experimental apparatus is presented by Theocaris [8] and Durelli and Parks [9].

The original technique developed by Ligtenberg and the subsequent improvements have enabled the partial slopes to be determined directly by a photograph. However, there are some limitations in these methods which restrict their use. The plate must be initially flat; otherwise, fringes will occur due to the inital curvature of the plate. For example, black Plexiglas is an excellent material to use in the Ligtenberg method because of the good surface quality. A polished aluminum plate has enough surface variation to cause many initial fringes. The use of partial mirrors in the system reduces the available light to the camera which is a limitation when high-speed cameras are used to photograph a dynamic event. Also, double exposures are difficult for dynamic events.

To determine the response of flat plates subjected to blow-off, a projected grid method was utilized because of the limitations of the more direct Moire' methods. A rotating drum camera was used to record the event with light illumination provided by a pulsed light source of approximately 8.6-msec time duration. However, all of the avaliable light was needed to expose the film and proper film exposure could not be obtained with the Ligtenberg techniques.

In the reflecting grid method of analysis, the data reduction is generally more difficult than the Moire' methods. However, if analysis is restricted to the maximum conditions at the center of the plate, then the amount of work is considerably reduced. Although data are recorded for the complete response of the plate, only the maximum conditions are included in this report.

II. THEORY

A. General

The principle of the method used to record slope contours in thin plates is shown schematically in Figure 1. A light field is used to reflect a grating onto the reflective surface of an initially flat plate. After deformation, the camera records the distorted grid pattern reflected by the deformed plate.

Refer to Figure 2 and let a point a' on the undeformed plate reflect light from a point y_3 on the grid illuminated by collimated light at an incident angle α. When the plate is deformed, point a' reflects light from a point y_4 on the grid. When the plate is deformed, the angle of rotation of the plate at point a' is denoted by β. The angle β can be calculated from the change in shape of the grid pattern.

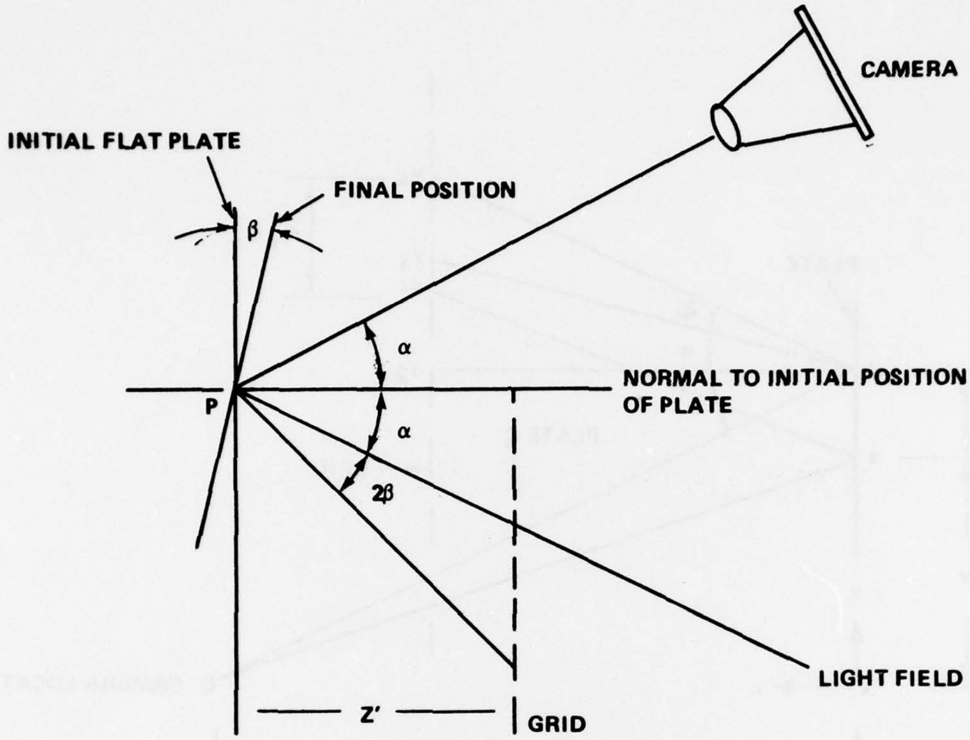

Figure 1. Schematic representation of apparatus used to obtain the partial slopes in flat plates.

From the geometry of the schematic of the experimental apparatus, the target of the angles ($\alpha + 2\beta$) and α can be calculated as

$$\tan(\alpha + 2\beta) = \frac{y_4 - y_2}{z'} \tag{1}$$

$$\tan(\alpha) = \frac{y_3 - y_2}{z'} \tag{2}$$

From the geometry of the experimental configuration, the following relationships are known:

$$y_2 = y + D_y \tag{3}$$

$$y_4 = y_1 + N_y G_y \tag{4}$$

$$y_3 = (y + D_y)\left[\frac{z' + z}{z}\right] \tag{5}$$

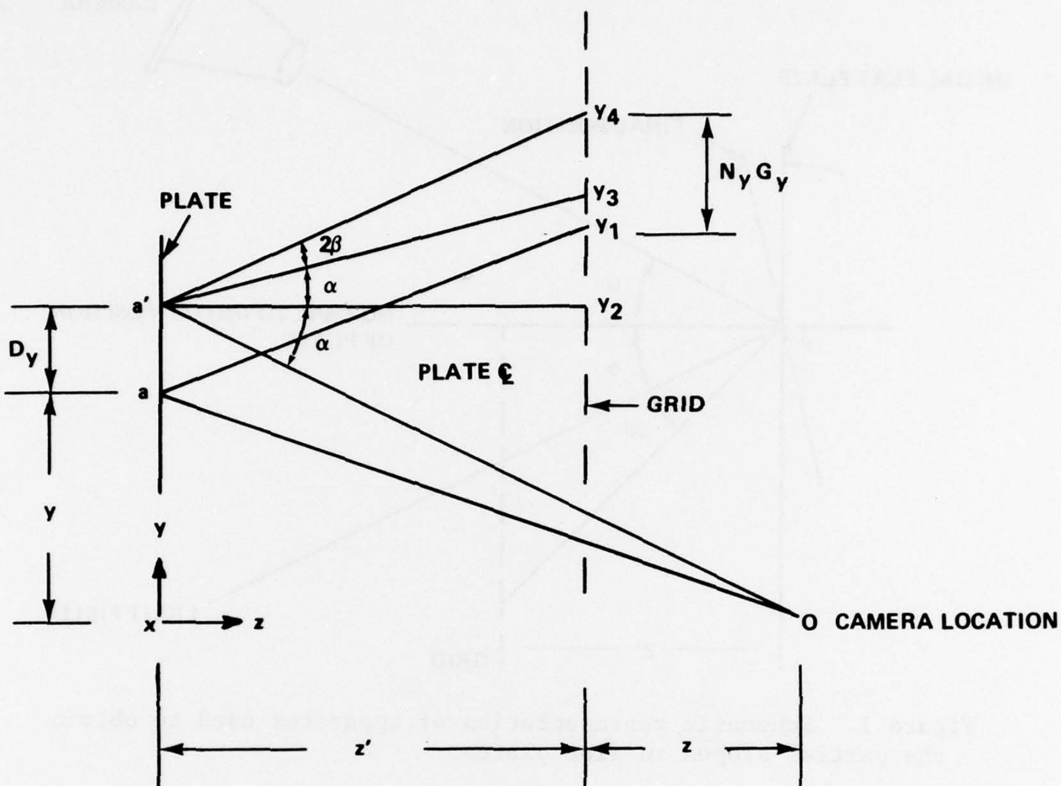

Figure 2. Experimental geometry for the blow-off simulation of a flat plate.

where

a = plate center

G_y = grid spacing in the y direction

N_y = number of grids between a' and a

β = slope at the point a' .

Equations (1) through (5) can be used to solve for the slope of the plate a' which has the following form:

$$\beta = \frac{1}{2}\left\{\tan^{-1}\left[\frac{N_y G_y}{z'} + \frac{y}{z} - \frac{D_y}{z'}\right] - \tan^{-1}\left[\frac{y}{z} + \frac{D_y}{z}\right]\right\} \quad . \tag{6}$$

Equation (6) is the basic equation which relates the slope of the plate at point a' to the change in grid spacing. This equation can be simplified for small deformation approximations consistant with the linear plate theory. However, in the analysis of the data, Equation (6) will be used in the general form.

B. Restrictions for Small Angle Changes

The results for tan 2β in Equation (6) can be simplified based on small angles of rotation approximations. The angle β in Equations (1) and (2) can be put in the following form consistant with these restrictions:

$$\tan(2\beta) = \left\{\frac{y_4 - y_2}{z'}\right\}\left\{1 - \tan(\alpha)\tan(2\beta)\right\} - \tan(\alpha) \tag{7}$$

The term $(y_4 - y_2)/z'$ can be put in the following form:

$$\frac{y_4 - y_2}{z'} = \frac{y_4 - y_3}{z'} + \tan\alpha \quad . \tag{8}$$

Equations (7) and (8), with the restriction that usually in an experiment $y_4 - y_3 \ll z'$, can be reduced to

$$\beta \simeq \frac{(y_4 - y_3)\cos^2\alpha}{2z'} \quad . \tag{9}$$

Equation (9) in this restricted form agrees with the methods used by Theocaris [8] and Durelli and Parks [9].

Figure 3 illustrates the coordinate system and location of the projected grid orders on the flat plate. A reference mark was projected on the surface of the plate to locate the plate centerline of the x_o and y_o grid orders. Positive and negative grid orders will correspond to the positive and negative coordinate directions.

C. Stress-Strain-Displacement Relationships for Linear Plate Theory

In classical plate theory, the strain components are related to the transverse displacement w(x,y,t) and the in-plane components u(x,y,t), v(x,y,t) as shown in the following equations:

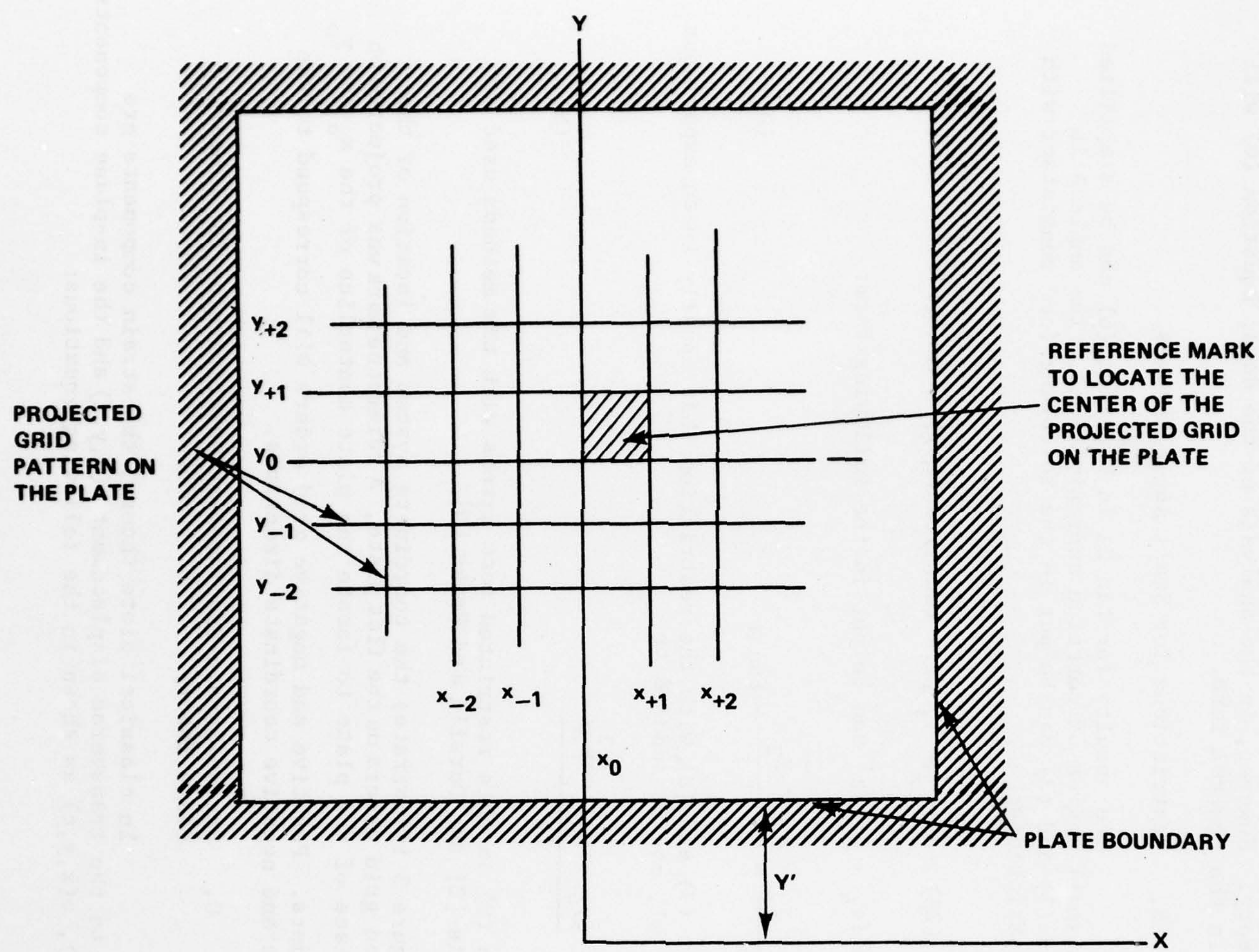

Figure 3. Coordinate system and orientation of the projected grid and orders on the plate surface.

$$\epsilon_{xx} = \frac{\partial u}{\partial y} - z \frac{\partial^2 w}{\partial x^2}$$

$$\epsilon_{yy} = \frac{\partial v}{\partial y} - z \frac{\partial^2 w}{\partial x^2} \qquad (10)$$

$$\gamma_{xy} = \frac{\partial u}{\partial y} + \frac{\partial v}{\partial x} - 2z \frac{\partial^2 w}{\partial x \partial y}$$

The nonzero stress components are related to the strain components as shown by the following equations:

$$\sigma_{xx} = \frac{E}{1 - \nu^2} [\epsilon_{xx} + \nu \epsilon_{yy} - (1 + \nu)\alpha\Delta T]$$

$$\sigma_{yy} = \frac{E}{1 - \nu^2} [\epsilon_{yy} + \nu \epsilon_{xx} - (1 + \nu)\alpha\Delta T] \qquad (11)$$

$$\tau_{xy} = \frac{E}{2(1 + \nu)} \gamma_{xy} ,$$

where

u, v, and w = displacements in the x, y, and z coordinate direction, respectively,

ϵ_{xx} = strain in the x-direction

ϵ_{yy} = strain in the y-direction

γ_{xy} = shearing strain

σ_{xx} = stress in the x-direction

σ_{yy} = stress in the y-direction

τ_{xy} = shearing stress

α = coefficient of linear expansion

ΔT = differential temperature

ν = Poisson's ratio.

III. EXPERIMENTAL GEOMETRY AND METHOD OF LOAD APPLICATION

A. Plate Foil Sublimation Experiments

Initial experiments were conducted to test the proposed plate-foil design. The aluminum plate design is shown in Figure 4(a), where an alummum foil is bonded to a dielectric layer which is bonded to the aluminum plate test specimen. This geometry worked very well; however, some difficulties were encountered which restricted the eventual use of this configuration. The reflecting surface of the plate could not be polished so that a highly reflecting flat surface could be obtained. When a rectangular grid was projected on the surface of this plate, the reflected pattern was distorted. The polished surface did not reflect enough light to expose the film properly.

A plate geometry, as shown in Figure 4(b), was made and tests were conducted to determine the reflecting surface characteristics. This surface produced very good results. In addition, fabrication of the models was simplified. The model consists of a clear Plexiglas plate which has been painted on one side with a flat black lacquer paint. Aluminum foil of 99% purity is then bonded to the painted surface using a rubber cement compound. The black surface allows the front surface of the plate to reflect light in a very efficient manner and serves as a mask for the light generated when the foil sublimates.

B. Exploding Foil Experiments

Blow-off simulation of the flat plate was determined by sublimating the aluminum foil with a high energy capacitor discharge unit.

The electrical design of the equipment of this system is presented in detail in a report by Cost et al. [10]. Basically, the system consists of an 18,600-J high energy capacitor discharge unit of low inductance electrical energy capable of delivering rapid pulses of intense electrical currents. The unit has a main capacitor bank which consists of a six 60-μf capacitors in parallel producing a combined capacity of 360 μf. The main bank is charged from a high voltage power supply which uses a conventional 115-V 60-cycle ac power supply and a high voltage secondary unit consisting of four No. 8020 tubes in a bridge rectifier circuit. Foil sublimation is accomplished by mounting the flat plate and foil (Figure 4) in a mounting device as shown in Figure 5. The foil contacts the electrodes and sublimates when the electrical energy is discharged in the foil. Initial electrode design, as shown in Figure 5, did not produce a uniform sublimation of the foil. Results of this design are shown in Figure 6. The corners of the plate did not sublimate and the high speed photographs shown in Figure 6 indicate a nonuniform sublimation of the foil.

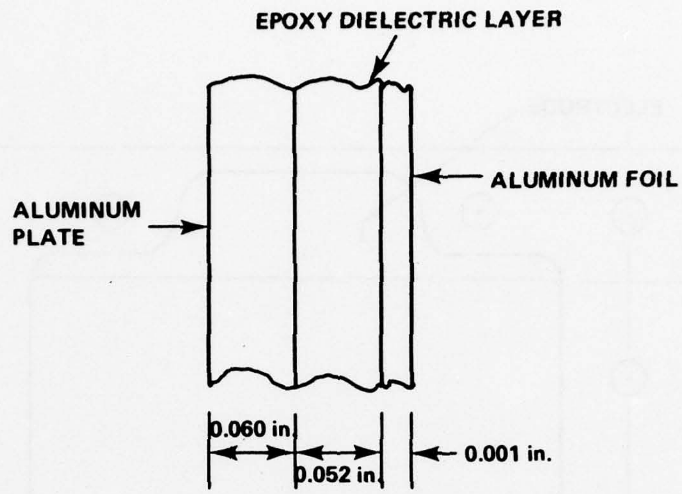

Figure 4(a). Aluminum plate with dielectric layer and foil backing.

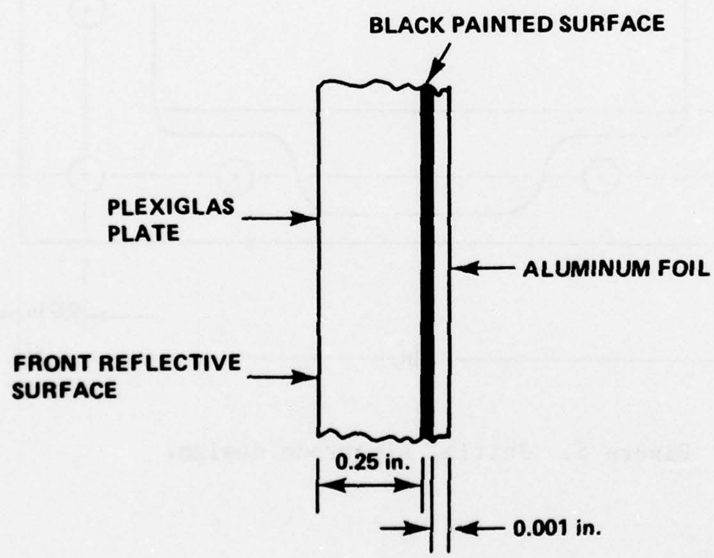

Figure 4(b). Plexiglas plate with aluminum foil backing.

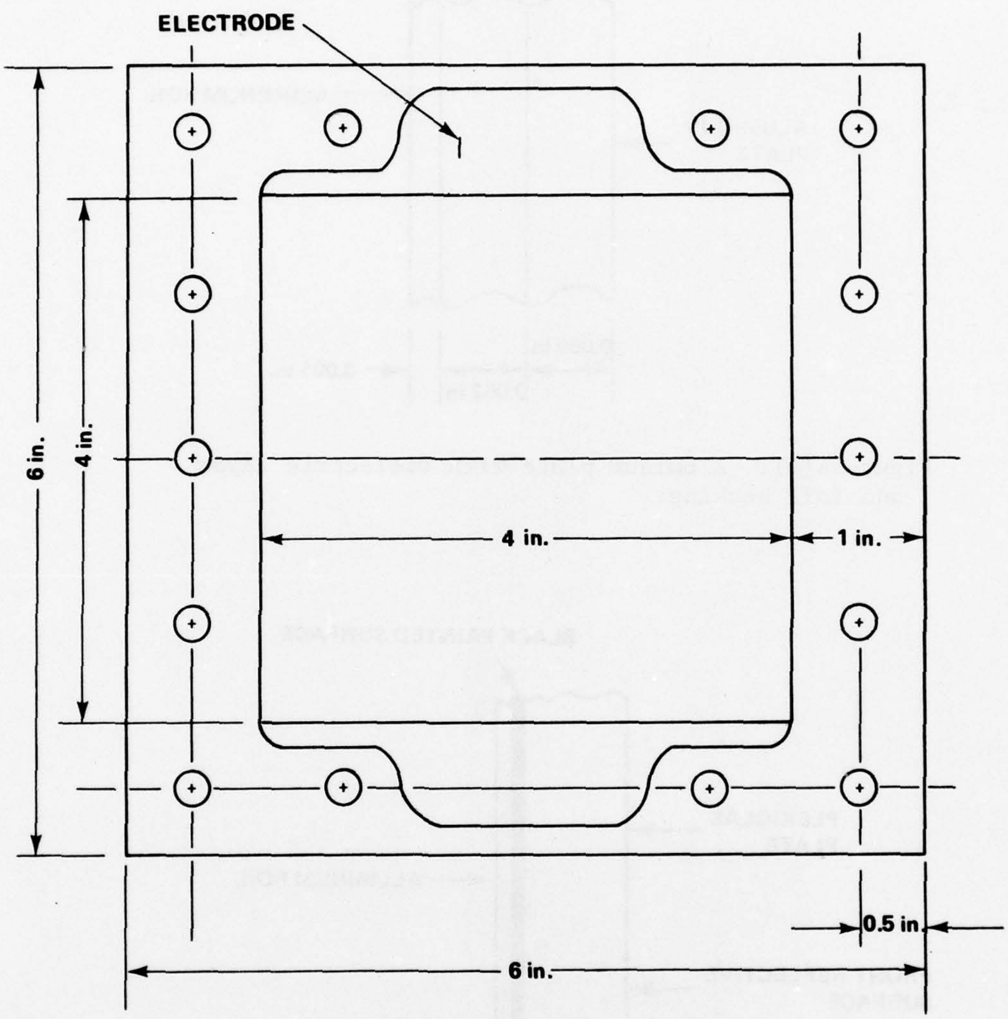

Figure 5. Initial electrode design.

Figure 6. High speed photograph of sublimation process with the initial electrode design.

Redesign of the electrodes is shown in Figure 7. Basically, the only difference is that the electrodes make contact along the edge of the foil instead of a small area at the plate edge. The plate holding fixture is made of G-10 phenolic which is a good insulator. This fixture has produced very good results which are illustrated in Figure 8. Also a high speed photograph of the foil sublimation is shown in Figure 8. A test of a 4 × 4 × 0.001-in. aluminum foil with a capacitor bank voltage of 7500 V was conducted. The high speed camera was operated at a framing rate of 3000 frames/sec. The sublimation time of the foil was measured from the photographic data to be 0.0159 sec.

C. Impulse Calculations

Prior research [11] presented indicates that an acceptable model for the impulse derived from the sublimation of an aluminum foil on an insulative substrate is given as:

$$I_\beta = 9150\ \rho h\ (E_d - E_s)^{0.5} \tag{12}$$

where

I_β = impulse (Taps/cm^2)

E_d = capacitor bank energy discharge (Cal/gm)

E_s = sublimation energy of foil (Cal/gm)

ρ = density of foil (gm/cm^3)

h = foil thickness (cm).

Using a density of $\rho = 2.702$ gm/cm^3 for aluminum evaluated to be approximately 99% pure by mass spectroscopy, the following relations hold true:

$$\text{1-mil foil:}\quad I_\beta = 62.797\ (60.727\ V^2 - E_s)^{0.5} \tag{13}$$

$$\text{0.5-mil foil:}\quad I_\beta = 31.399\ (121.4597\ V^2 - E_s)^{0.5} \tag{14}$$

$$\text{0.25-mil foil:}\quad I_\beta = 15.699\ (242.919\ V^2 - E_s)^{0.5} \tag{15}$$

where

V = Capacitor bank voltage level (kv)

E_s = 3200 (cal/gm)

I_β = impulse (Taps/cm^2)

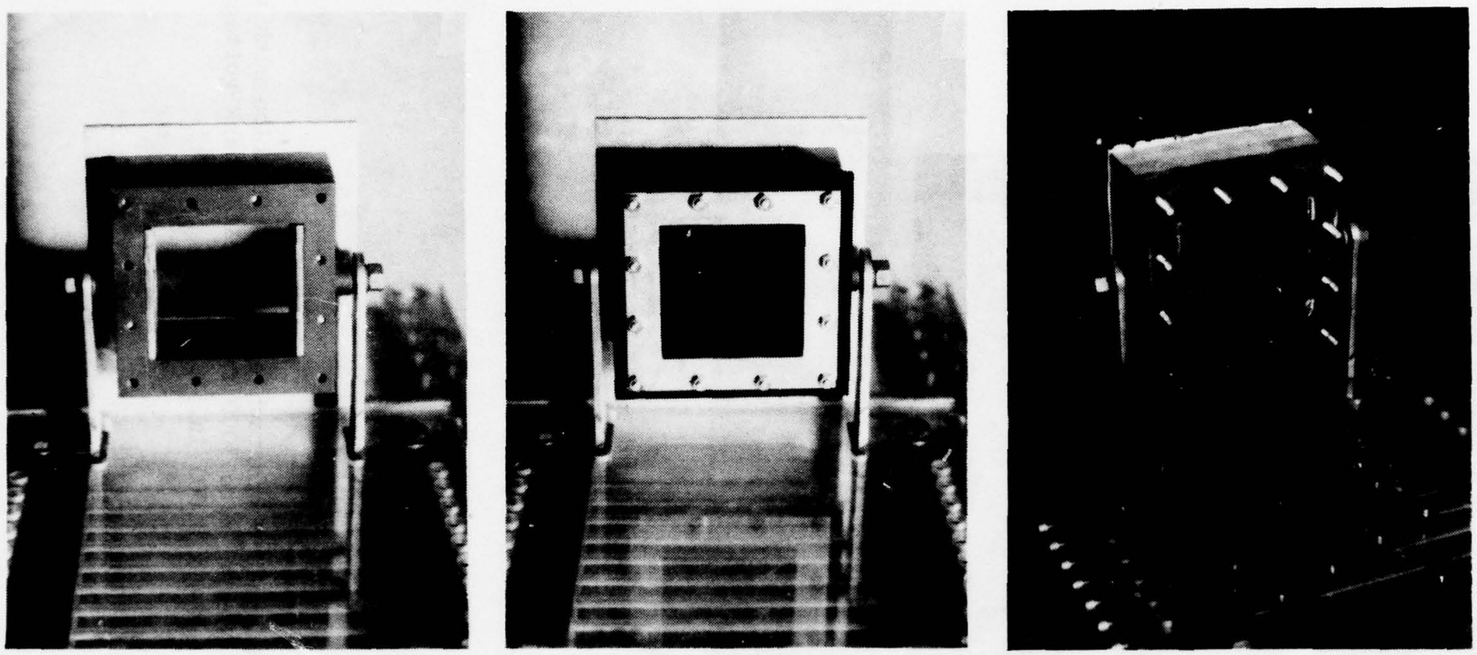

(a) (b) (c)

Figure 7. (a) Redesign of electrodes and mounting fixture; (b) Plate specimen loaded in the test fixture; (c) Complete sublimation of the foil in the redesigned fixture.

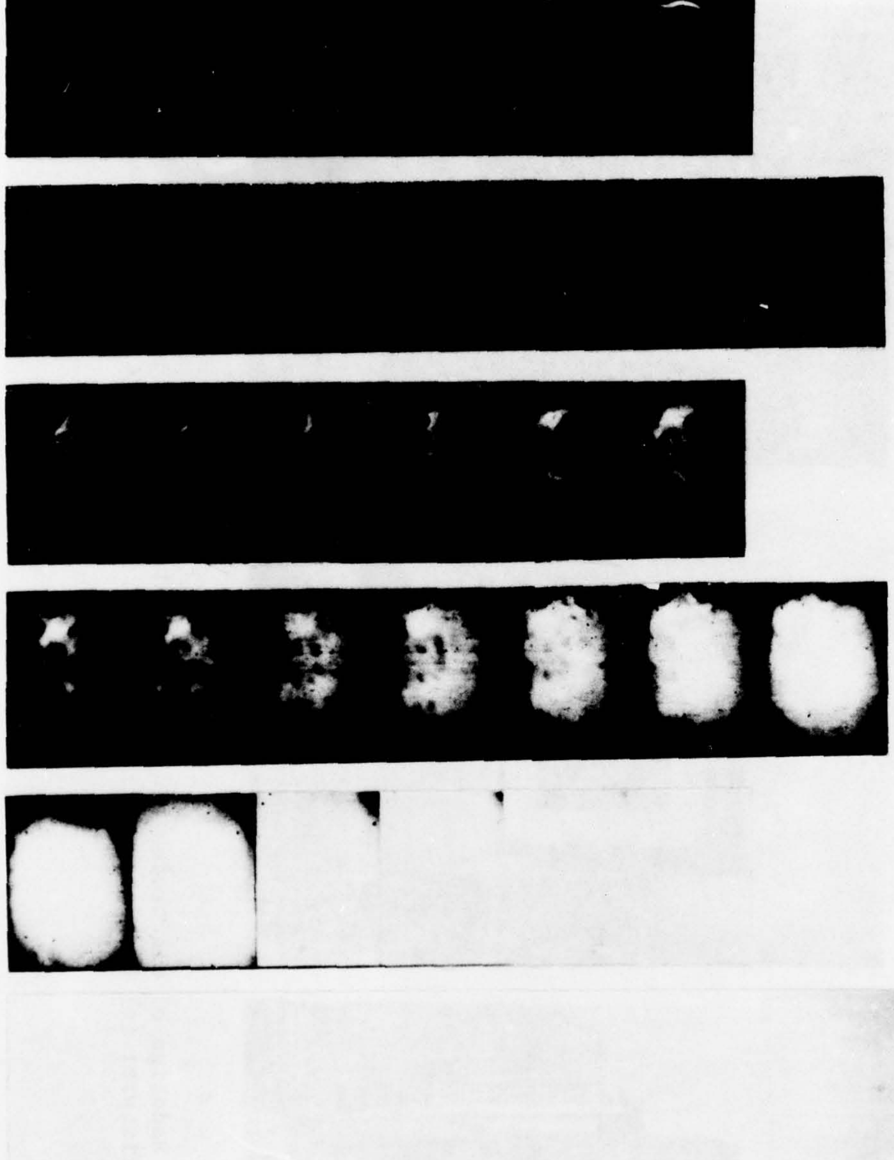

Figure 8. High speed photograph of foil sublimation with redesigned electrodes (framing rate 3000 fps, capacitor bank voltage – 7500V, foil area - 4 × 4 × 0.001 in.).

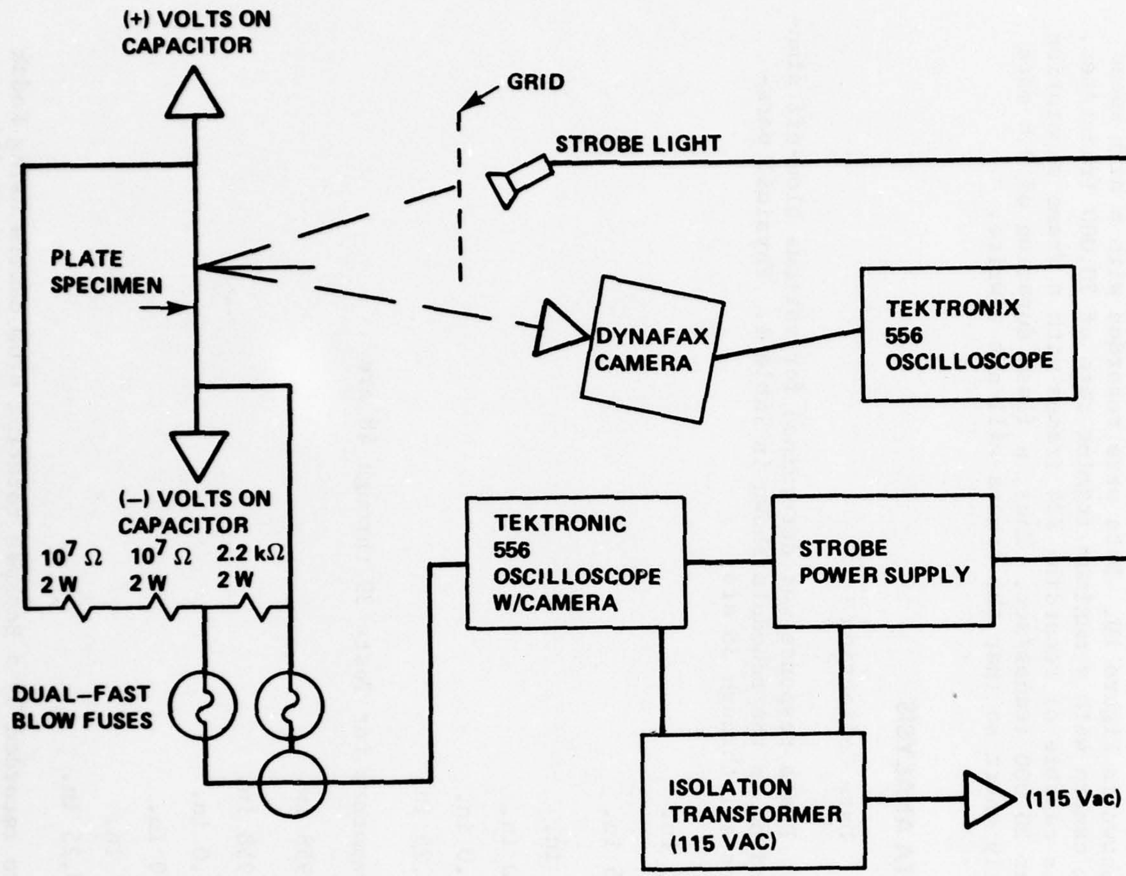

Figure 9. Schematic diagram for triggering the strobe light source with the exploding foil.

D. Experimental Geometry and Timing of the Event

The experimental arrangement used for the timing of the sequence of events in the exploding of the foil and data recording is shown in Figures 9 and 10. A voltage divider is attached across the electrodes of the exploding foil test fixture whose output is used to trigger a Beckman electronic flash through an oscilloscope. A complete assembly is shown in Figure 10. Data were recorded with a high speed rotating drum camera with a maximum framing rate of 20,000 frames/sec. This camera is capable of recording 224 frames with a frame separation of 39 μsec at 20,000 frames/sec. Thus, a flash duration of 8.6 msec is sufficiently short so that the camera will not rewrite.

IV. DATA ANALYSIS

A. Data Collection

Plate response was determined for various blow-off simulations according to the schedule shown in Table 1. Physical parameters for Tests 1 through 38 are

$G_x = 0.5$ in.

$G_y = 0.5$ in.

$x = 11$ in.

$y = 0.0$ in.

$z = 32.0$ in.

$z' = 19.25$ in.

Physical parameters for Tests 39 through 48 are

$G_x = 0.958$ in.

$G_y = 0.958$ in.

$x = 11.0$ in.

$y = 0.0$ in.

$z = 32$ in.

$z' = 19.25$ in.

All data were recorded by a Beckman rotating drum camera using Kodak 2475 recording film. The camera speed for all tests was 17,800 frames/sec. Plate response illustrating the shape of a deformed grid for a typical test is shown in Figure 11.

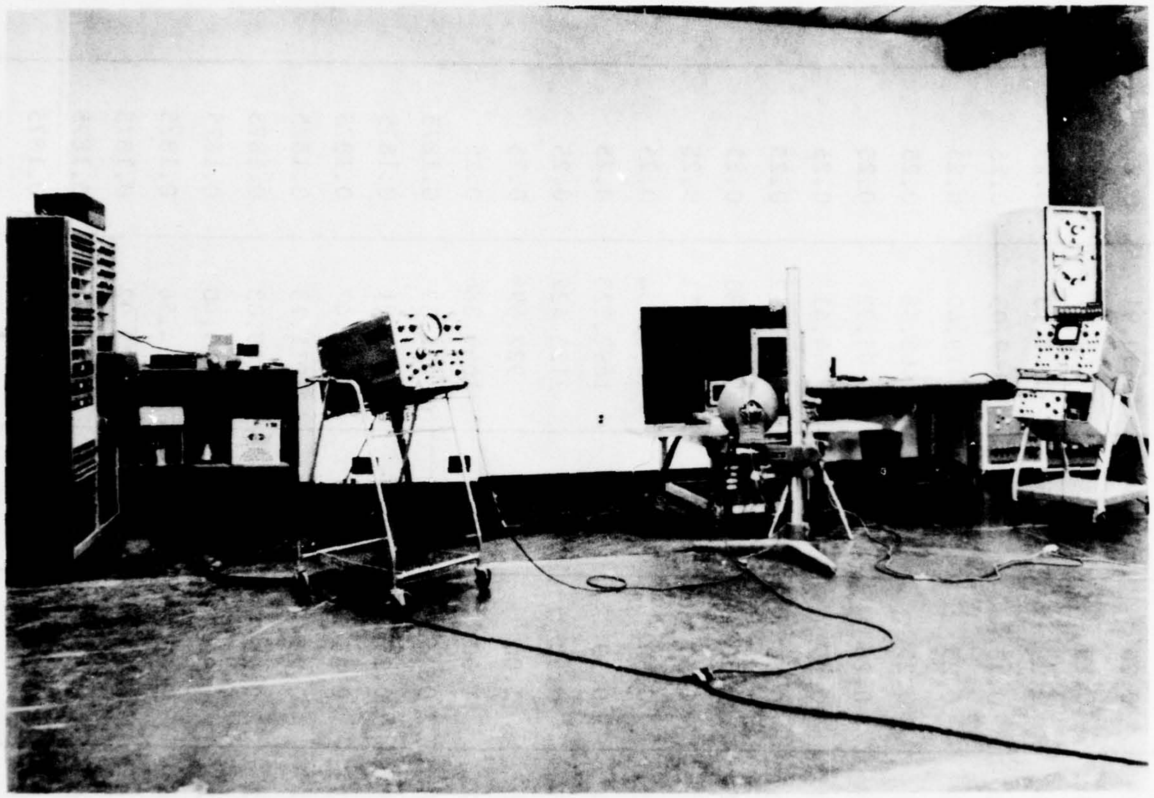

Figure 10. Experimental configuration.

TABLE 1. EXPLODING FOIL TEST SCHEDULE

Test No.	Foil Thickness (mil)	Voltage Level (kV)	Impulse (Taps/cm^2)	Plate Thickness (in.)
1	0.25	4.0	411.39	0.25
2	0.25	4.5	650.91	0.25
3	0.25	5.0	841.47	0.25
4	0.25	5.5	1011.13	0.25
5	0.25	6.0	1169.03	0.25
6	0.25	6.5	1319.40	0.25
7	0.25	7.0	1465.56	0.25
8	0.25	7.5	1605.92	0.25
9	0.25	8.0	1744.41	0.25
10	0.50	5.5	683.717	0.25
11	0.50	6.0	1075.180	0.25
12	0.50	6.5	1380.011	0.25
13	0.50	7.0	1647.034	0.25
14	0.50	7.5	1892.323	0.25
15	0.50	8.0	2123.422	0.25
16	1.00	7.5	922.696	0.25
17	1.00	8.0	1645.386	0.25
18	0.25	4.0	411.39	0.1875
19	0.25	4.5	650.91	0.1875
20	0.25	5.0	841.47	0.1875
21	0.25	5.5	1011.13	0.1875
22	0.25	6.0	1169.03	0.1875
23	0.25	6.5	1319.40	0.1875
24	0.25	7.0	1464.56	0.1875
25	0.25	7.5	1605.92	0.1875
26	0.25	8.0	1744.41	0.1875
27	0.50	5.5	683.717	0.1875
28	0.50	6.0	1075.180	0.1875
29	0.50	6.5	1380.011	0.1875

TABLE 1. (Concluded)

Test No.	Foil Thickness (mil)	Voltage Level (kV)	Impulse (Taps/cm^2)	Plate Thickness (in.)
30	0.50	7.0	1647.034	0.1875
31	0.50	7.5	1892.323	0.1875
32	0.50	8.0	2123.422	0.1875
33	1.00	7.5	922.696	0.1875
34	1.00	8.0	1645.386	0.1875
35	0.25	4.0	411.39	0.125
36	0.25	4.5	650.91	0.125
37	0.25	5.0	841.47	0.125
38	0.25	5.5	1011.13	0.125
39	0.25	4.0	411.39	0.125
40	0.25	4.5	650.91	0.125
41	0.25	5.0	841.47	0.125
42	0.25	5.5	1011.13	0.125
43	0.25	6.0	1169.03	0.125
44	0.25	6.5	1319.40	0.125
45	0.25	7.0	1464.56	0.125
46	0.25	7.5	1605.92	0.125
47	0.25	8.0	1744.41	0.125
48	0.25	8.0	1744.41	0.125

NOTES: On tests No. 38, 47, and 48, the plate failed under the test conditions and data were not recorded for analysis. Figure 12 shows the failure mode of Test No. 47.

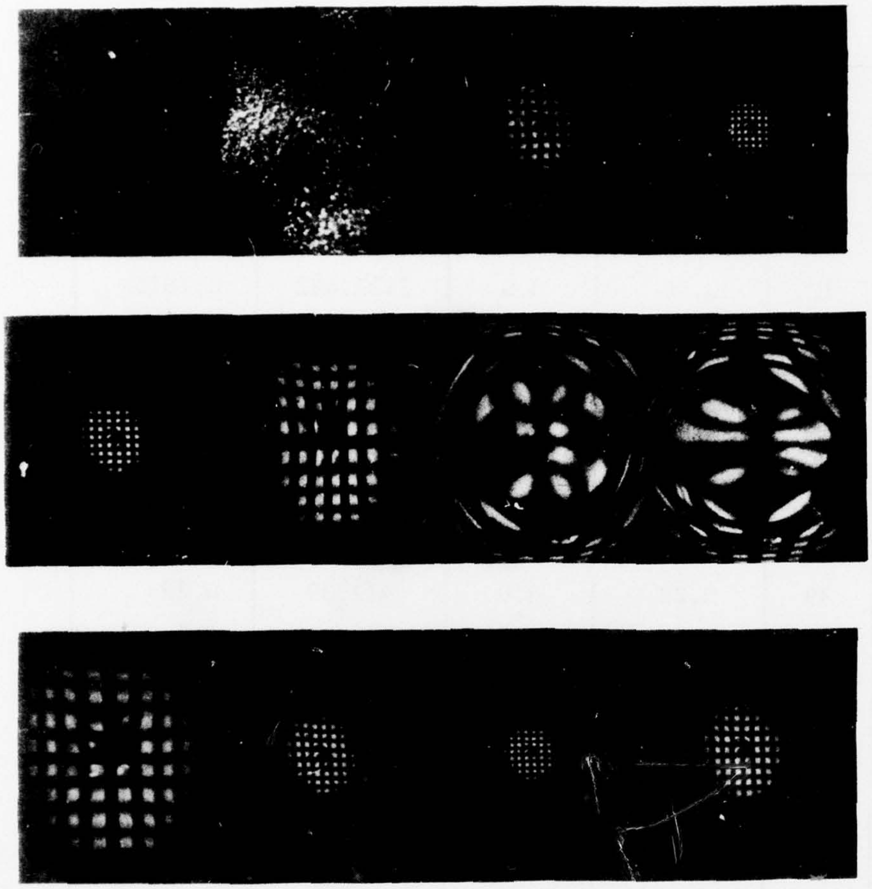

Figure 11. Plate responses for test No. 23.

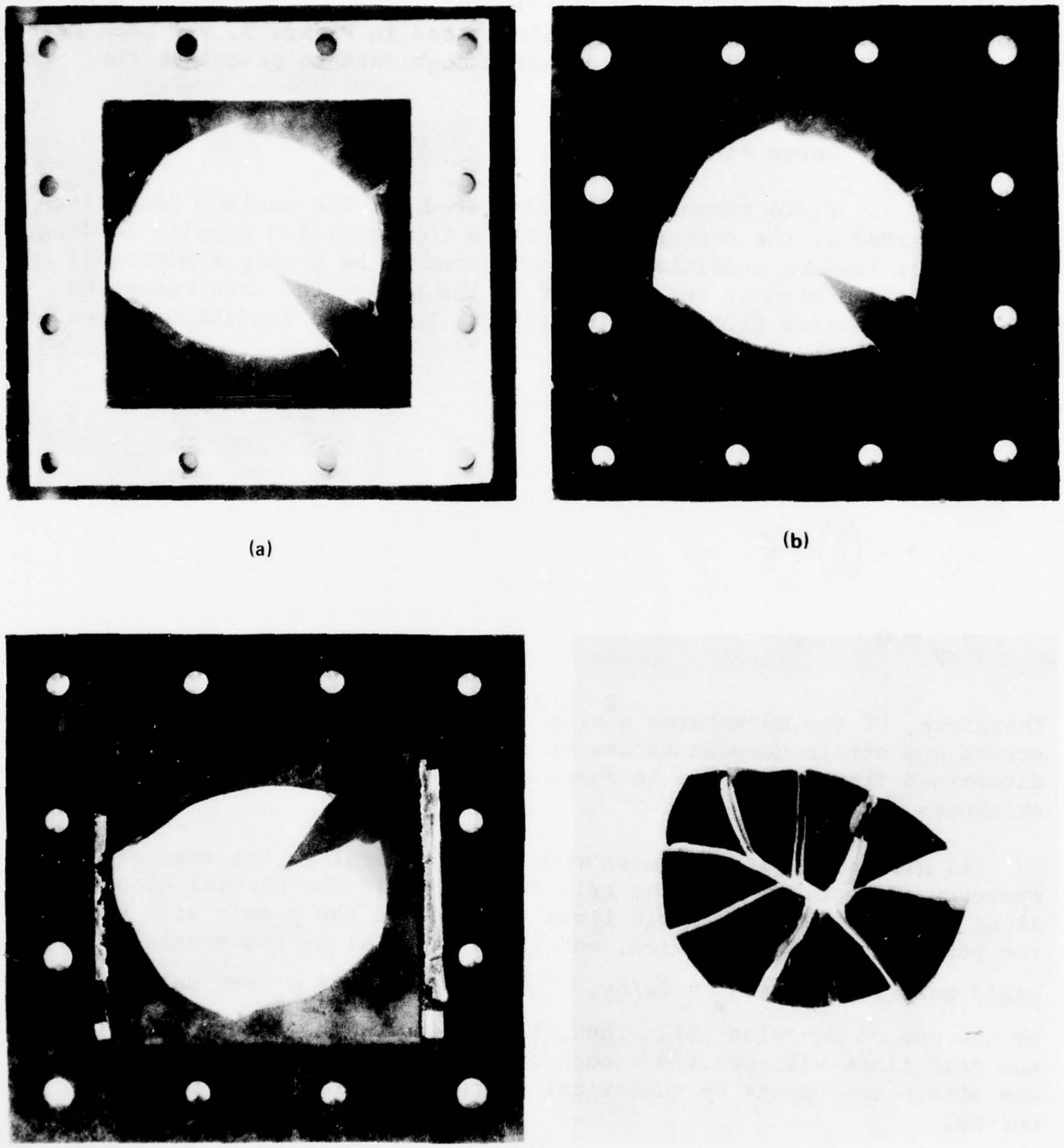

Figure 12. Failure of test No. 47: (a) specimen with clamp holder, (b) specimen without clamp holder, (c) sublimated side of specimen, (d) fragments of broken specimen.

Data for each test are tabulated in the Appendix. The location of the grid orders is denoted as X_{-2}, X_{-1}, X_o,... . Each subscript will denote the assigned grid order as illustrated in Figure 3. In each test, several frames were analyzed to obtain enough data to calculate the maximum strains.

B. Curve Fit Analysis

Plate response was calculated for the maximum conditions which occurred at the center of the plate for specified impulse loading. Because the loading conditions were observed to be nearly symmetrical and data were calculated at the midpoint of the plate, the data reduction and use of Equation (10) were simplified. For these conditions, Equations (10) reduce to the following form:

$$\epsilon_{xx} = -\left(\frac{h}{2}\right)\frac{\partial^2 w}{\partial x^2}$$

$$\epsilon_{yy} = -\left(\frac{h}{2}\right)\frac{\partial^2 w}{\partial y^2} \qquad (16)$$

$$\gamma_{xy} = 0 \quad .$$

Therefore, if the curvatures $\partial^2 w/\partial x^2$ amd $\partial^2 w/\partial y^2$ are known, then the stress and strain components can be calculated and curvatures are determined from the change in shape of the grid lines where the plate thickness h is known.

If grid lines are oriented with lines parallel to the axes of symmetry (Figure 3), then the grid changes yield the partial slopes along each of the axes. Grid lines parallel to the y-axis will yield the partial slopes $\beta_x = \partial w/\partial x$, and lines parallel to the x-axis will yield partial slopes $\beta_y = \partial w/\partial y$. The slopes β_x and β_y are calculated by the use of Equation (6). Then, in principle, the change in shape of the grid lines will provide enough experimental information to calculate the strain components by numberical differentiation of the β_x and β_y curves.

Because the data can be approximated as symmetrical with respect to the midpoint of the plate, $\partial w/\partial x = \partial w/\partial y = 0$; therefore, $\beta_x = \beta_y = 0$ at the plate center. Plate curvatures $\partial^2 w/\partial x^2$ and $\partial^2 w/\partial y^2$ were evaluated by fitting a cubic spline through the grid order data. The cubic spline has the form

$$\beta_x = a_1 x + a_2 x^2 + a_3 x^3 . \qquad (17)$$

A difference function was then formed as defined by the following equation:

$$\sum \delta_i^2 = \sum \left[\beta_x i - (a_1 x_i + a_2 x_i^2 + a_3 x_i^3) \right]^2 \tag{18}$$

when the x_i, β_i are the input data. Constants a_i are determined from a minimization of the difference function as defined by

$$\frac{\partial \sum \delta_i^2}{\partial a_i} = 0 \tag{19}$$

Equations (15) can be put in the following form:

$$\begin{aligned} a_1 x_2 + a_2 x_3 + a_3 x_4 &= \beta_1 \\ a_1 x_3 + a_2 x_4 + a_3 x_5 &= \beta_2 \\ a_1 x_4 + a_2 x_5 + a_3 x_6 &= \beta_3 \quad , \end{aligned} \tag{20}$$

where

$$\begin{aligned} \sum x_i^k &= x_k \\ \sum x_i^k \beta i &= \beta \quad . \end{aligned} \tag{21}$$

Equations (15) were solved for the constants a_1, a_2, and a_3.

Plate curvature $\partial^2 w/\partial x^2$ can be evaluated from the data because $\partial^2 w/\partial x^2 = \partial \beta_x/\partial x|x = 0$ and from Equation (17) $\partial \beta_x/\partial x|x = 0 = a_1$. The curvature $\partial^2 w/\partial y^2$ at the plate center can be evaluated in a similar manner using the grid order data y_{-2}, y_{-1}, y_o, ...

C. Error Analysis

To study the plate deflections of a Plexiglas specimen, a high-speed camera operating at approximately 17,800 frames/sec was used. This results in a discrete sampling interval of approximately 0.0562 msec perframe. The period of free vibration for the 0.1875-in. plates is approximately 562 Hz while the 0.250-in. plates vibrate at approximately 500 hz. This means that approximately 20 to 40 frames of data can be obtained for one complete cycle of a plate vibrating freely using the specified sampling interval. However, it is still possible to

miss the point of maximum plate deflection because it can occur in any 0.0562-msec interval and be undetected by a high speed camera. This is one of the contributing factors of data scatter in this analysis.

Another factor of error in the analysis is due to locating the grid centers of the photographed plate deflections. Errors in locating the grid centers can be multiplied by a factor as large as five or six. To minimize this error, a photomicrometer was used at 20X power to digitize the grid centers of the deflection photographs.

Errors can also be made in centering the camera equipment and measuring the various distances used in the analysis. These errors are considered to be trivial when compared with discrete sampling errors and errors due to digitizing grid locations.

Finally, the sublimation phenomenon of a foil is a complex problem. Surface irregularities, poor electrode contact, atmospheric conditions, foil surface conditions, etc. will play a part in the scatter of the data. The electrical characteristics of the capacitor bank and electrical energy transport cables contribute significantly to the complexity of the problem. Irregularities in their characteristics contribute to data scatter. The total estimated error in the results when all of these factors are considered can be as great as 15% to 20%.

The only sources of error which can be adequately determined are due to errors in distance measurements and errors in digitizing the data. Distance measurement errors are estimated to be less than 1%. An indication of errors due to digitizing the film data can be made by comparing the values of ϵ_{xx} and ϵ_{yy} for the points of maximum strain. Theoretically, they should be equal assuming uniform loading conditions on the plates. It is observed from the computed results that ϵ_{xx} generally agrees with the ϵ_{yy} values within the experimental accuracy.

V. DISCUSSION AND RESULTS

Table 2 tabulates the results of Experiments 1 through 34. Each test shown gives the corresponding foil thickness, capacitor bank voltage, estimated plate impulse, and foil energy density. The maximum calculated values of the strain in both the x and y directions is given for the center of the plate.

Figures 13 through 16 indicate the theoretical plate strains of Plexiglas versus impulse level for a linearly decaying pressure profile [11]. The actual results for Tests 1 through 34 are shown in Figures 17 through 40. A cubic least square curve fit was applied to the laboratory data. The results are shown with each figure. These equations should be applied only over the experimental domain of the lab data. The results for strain versus impulse level are generally fairly

TABLE 2. RESULTS OF EXPERIMENTS 1 THROUGH 34

Test No.	Foil Thickness (mil)	Capacitor Voltage (kV)	Plate Impulse (taps/cm^2)	Foil Energy Density (cm/gm)	(cm/cm) $E_{xx_{MAX}}$	Plate Thickness (cm)	(cm/cm) $E_{yy_{MAX}}$
1	0.25	4.0	411.39	3886.704	0.003688	0.635	0.003904
2	0.25	4.5	650.91	4919.109	0.004556	0.635	0.003773
3	0.25	5.0	841.47	6072.97	0.004519	0.635	0.004462
4	0.25	5.5	1011.13	7348.30	0.004351	0.635	0.004178
5	0.25	6.0	1169.03	8745.08	0.006090	0.635	0.005131
6	0.25	6.5	1319.40	10263.3	0.005067	0.635	0.005599
7	0.25	7.0	1464.56	11903.03	0.006782	0.635	0.005558
8	0.25	7.5	1605.92	13664.19	0.006949	0.635	0.005971
9	0.25	8.0	1744.41	15546.81	0.009673	0.635	0.006760
10	0.50	5.5	683.717	3674.15	0.006297	0.635	0.005490
11	0.50	6.0	1075.180	4372.55	0.006586	0.635	0.005907
12	0.50	6.5	1380.011	5131.67	0.005916	0.635	0.005497
13	0.50	7.0	1647.034	5951.52	0.007762	0.635	0.006149
14	0.50	7.5	1892.323	6832.11	0.006821	0.635	0.006463
15	0.50	8.0	2123.422	7773.42	0.008212	0.635	0.007008
16	1.00	7.5	922.696	3415.91	0.006727	0.635	0.006261
17	1.00	8.0	1645.386	3886.55	0.008404	0.635	0.007083
18	0.25	4.0	411.39	3886.704	0.005430	0.476	0.005524
19	0.25	4.5	650.91	4919.109	0.005687	0.476	0.004819
20	0.25	5.0	841.47	6072.97	0.006867	0.476	0.005930

TABLE 2. (Concluded)

Test No.	Foil Thickness (mil)	Capacitor Voltage (kV)	Plate Impulse (taps/cm^2)	Foil Energy Density (cm/cm)	(cm/cm) $E_{xx_{MAX}}$	Plate Thickness (cm)	(cm/cm) $E_{yy_{MAX}}$
21	0.25	5.5	1011.13	7342.30	0.006327	0.476	0.005772
22	0.25	6.0	1169.03	8745.08	0.007727	0.476	0.007257
23	0.25	6.5	1319.40	10263.3	0.007088	0.476	0.006666
24	0.25	7.0	1464.56	11903.03	0.007833	0.476	0.007853
25	0.25	7.5	1605.92	13664.19	0.007876	0.476	0.006603
26	0.25	8.0	1744.41	15546.81	0.011150	0.476	0.009059
27	0.50	5.5	683.717	3674.15	0.008439	0.476	0.007887
28	0.50	6.0	1075.180	4372.55	0.010130	0.476	0.010390
29	0.50	6.5	1380.011	5131.67	0.009271	0.476	0.008564
30	0.50	7.0	1647.034	5951.52	0.008639	0.476	0.008314
31	0.50	7.5	1992.323	6832.11	0.008271	0.476	0.006612
32	0.50	8.0	2123.422	7773.42	0.009610	0.476	0.009267
33	1.00	7.5	922.696	3415.91	0.014070	0.476	0.009101
34	1.00	8.0	1645.386	3886.55	0.010450	0.476	0.008614

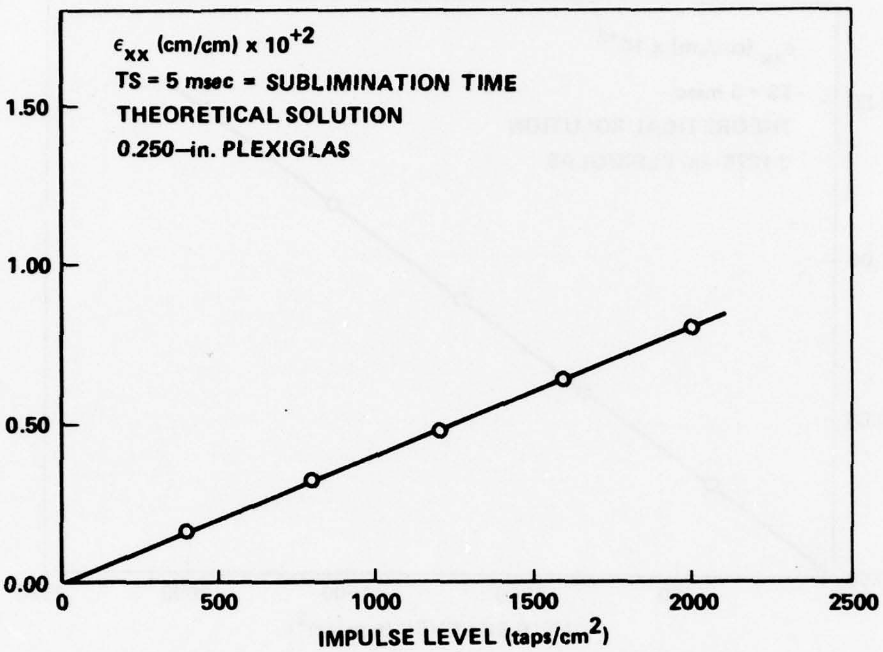

Figure 13. Theoretical plate strains.

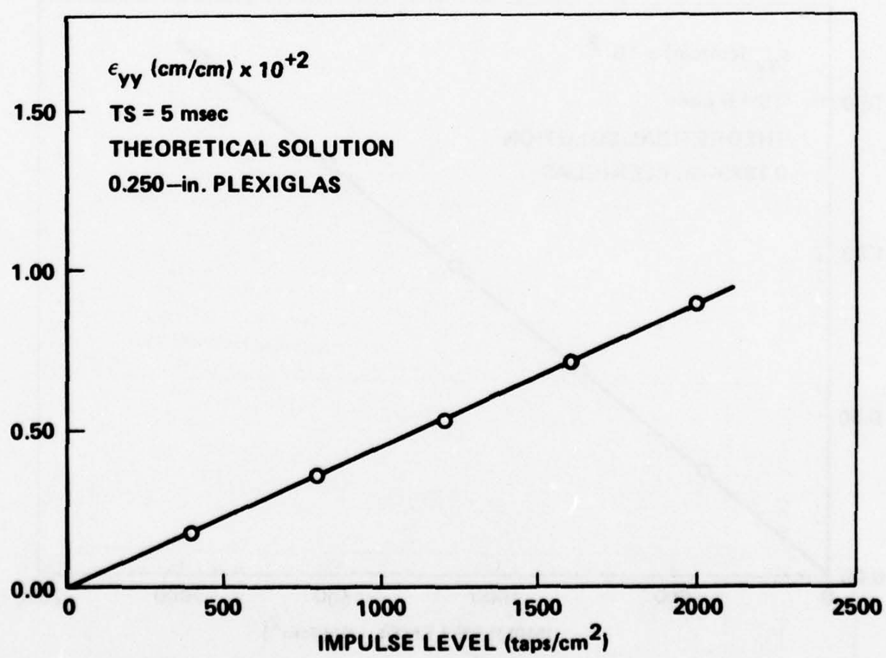

Figure 14. Theoretical plate strains.

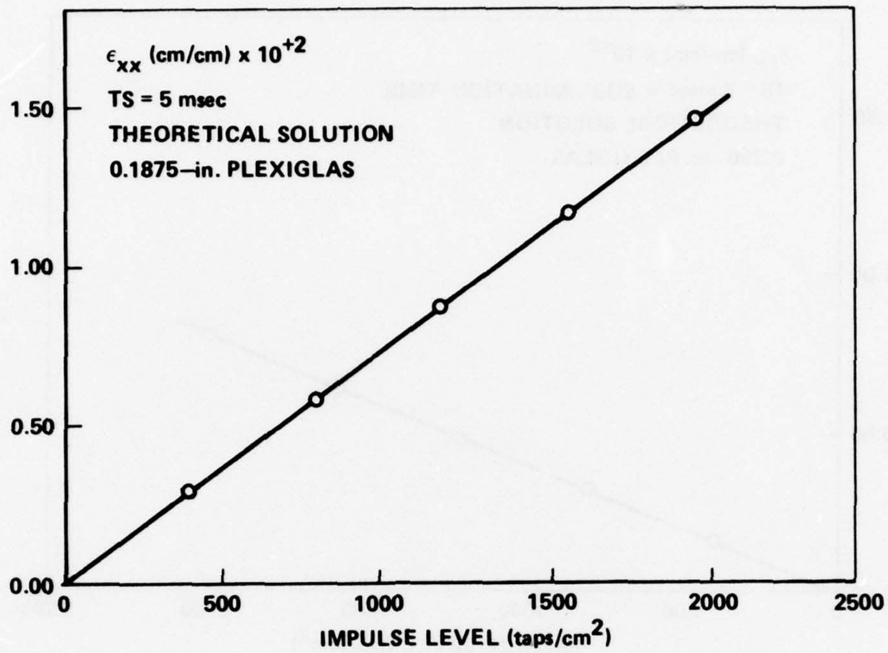

Figure 15. Theoretical plate strains.

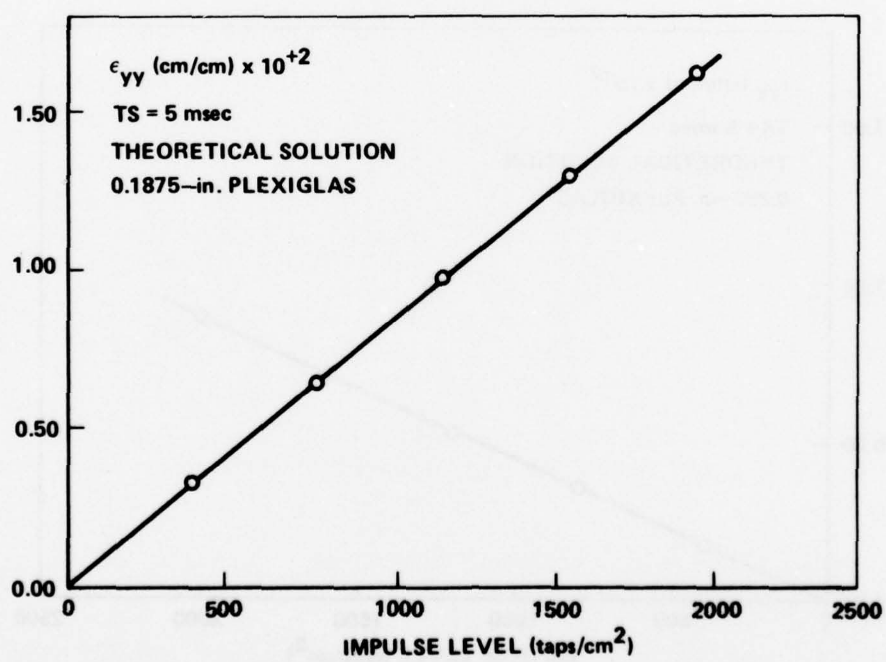

Figure 16. Theoretical plate strains.

linear which corresponds with the theoretical results. By adjusting the impulse level and impulse duration of the theoretical computer solution, the resulting theoretical curve can be forced to agree closely with the actual laboratory results. The experimental work described here indicates that the theoretical model for impulse due to foil sublimation is incomplete and requires some refinement. The curves for strain versus capacitor bank voltage level and foil energy density should be used in making predictions of plate response.

The strain versus impulse level curves indicate two possibilities: (1) the mathmatical model for impulse versus capacitor bank voltage is incorrect or (2) the computer equations for pressure versus time are incorrect. Although a mathmatical computer solution is desirable, it is not required because the curves for strain versus foil energy density are adequate. Figures 17 through 40 show that the plate strains are functions of foil thickness; for identical energy densities, thicker foils generally result in higher strain levels. The explanation for this may be the result of a high voltage skin effect on the foil.

VI. SUMMARY AND CONCLUSIONS

A technique to simulate and experimentally evaluate the effects of high concentrations of x-rays resulting from a nuclear detonation on missile structures was developed. Data from 34 tests were presented to demonstrate the technique. In these tests the effects of variations in the foil thickness, capacitor voltage, and plate thickness on the total impulse and maximum strain in the structure were determined.

The experimental error of these tests is estimated to be approximately 15% to 20%. However, this should not reflect on the technique because the major error source is the 17,800 frames/sec framing rate of the recording camera yielding a 0.281-msec interval for peak deflection to occur and not be recorded. To apply this technique, a framing rate of 50,000 to 100,000 frames/sec should be used; the experimental error should then be less than 10%.

Although the actual specimens used in the tests were made of Plexiglas, results for actual missile materials such as aluminum can be obtained through equations relating the material properties.

Four other tests were run on 0.318-cm thick Plexiglas specimen but the data were not valid because of excessive deflections and fracture of the specimen.

The results presented show that there is a strong indication that the sublimation phenomenon is a function of the following:

a) Foil geometry and material.

b) Electrical characteristics of the capacitor discharge device.

c) Electrical energy supplied to the foil.

d) Surface characteristics of the foil.

The contribution played by each of these factors and their correlation to an actual sublimation event require more detailed study to make an accurate estimation of the effects of a nuclear blast on a missile structure. The data curves indicate that foil energy density is not an entirely accurate estimation of structural performance although it does indicate certain trends. Considering the factors involved in the analysis of the data, it appears that given a known foil geometry, an accurate prediction of plate performance can be achieved for a given foil energy density. The smoothing effect of the least squares cubic spline curve fit to the experimental data should be used when data are taken from the experimental graphs.

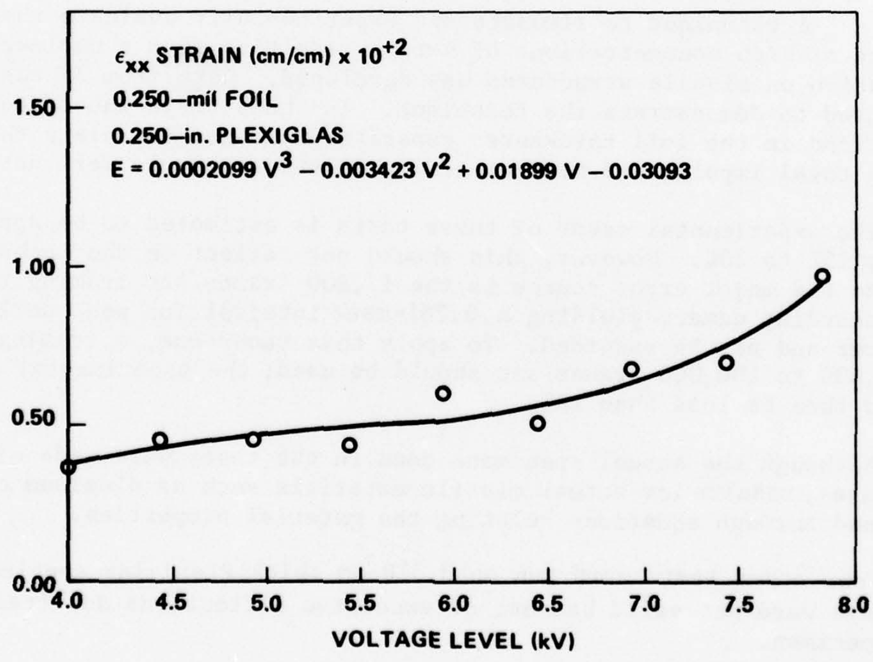

Figure 17. Plate strains as a function of foil thickness.

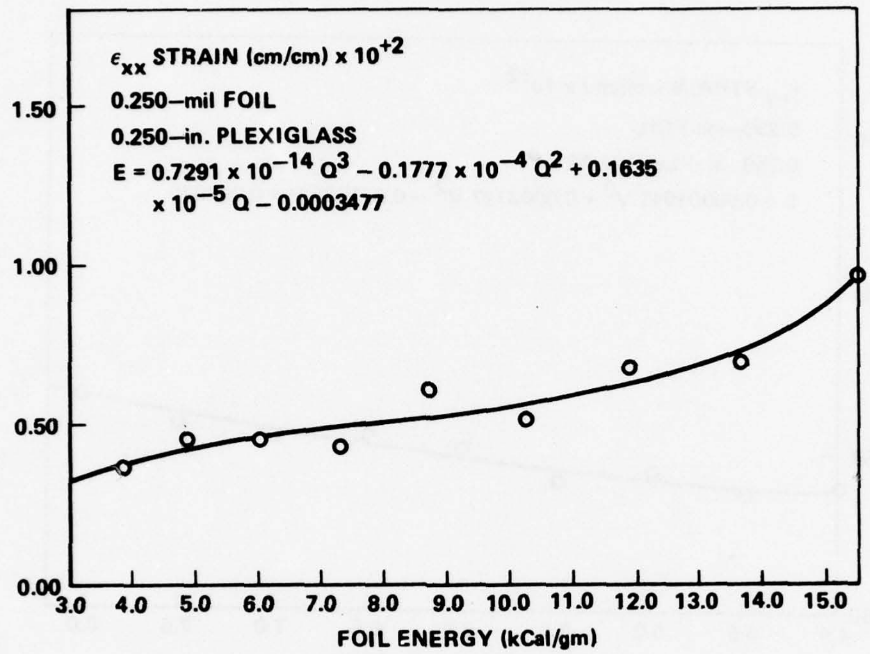

Figure 18. Plate strains as a function of foil thickness.

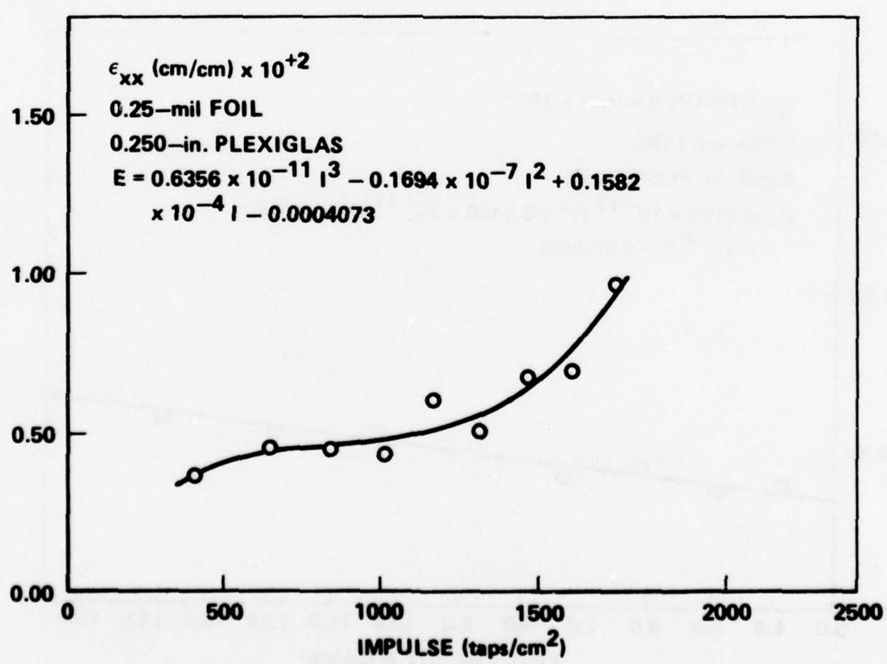

Figure 19. Plate strains as a function of foil thickness.

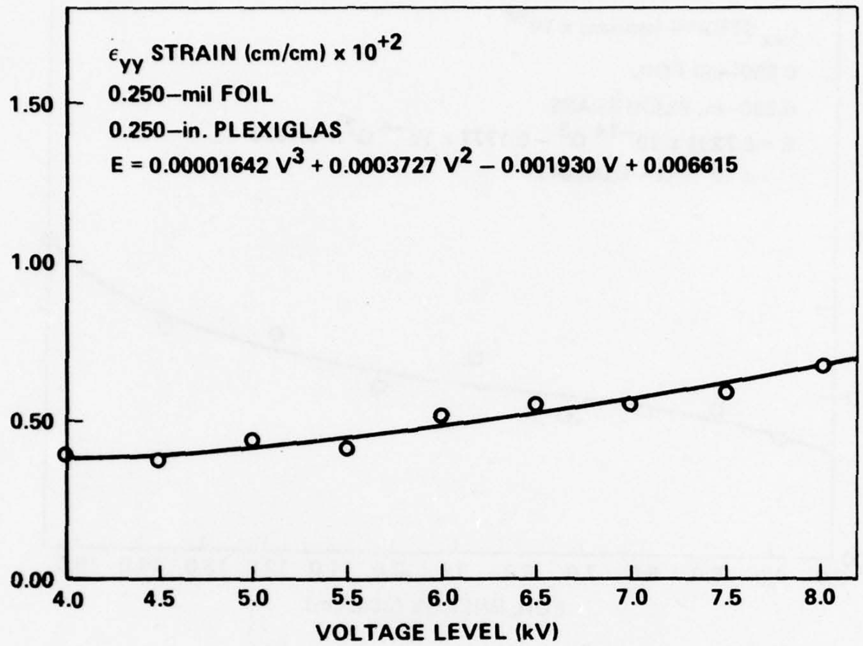

Figure 20. Plate strains as a function of foil thickness.

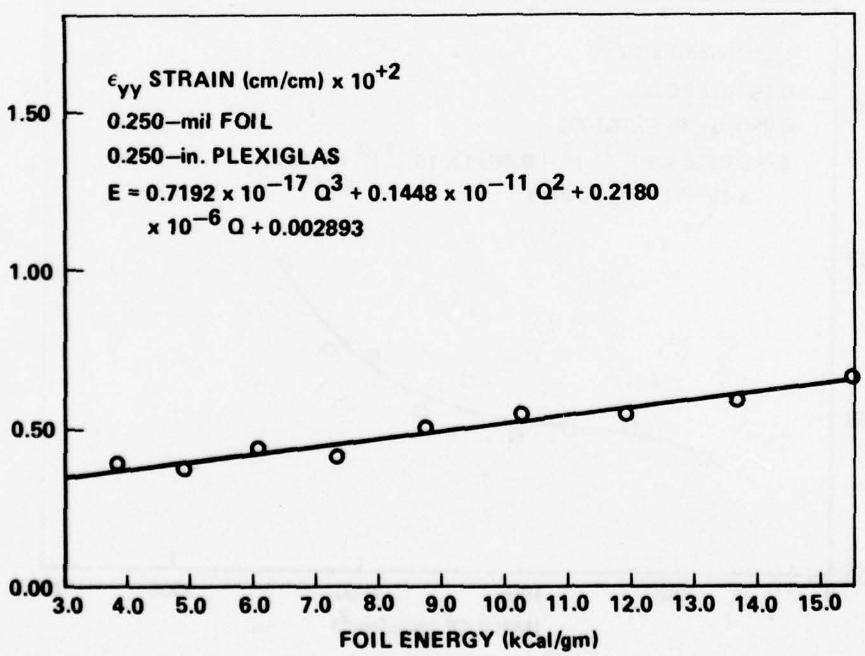

Figure 21. Plate strains as a function of foil thickness.

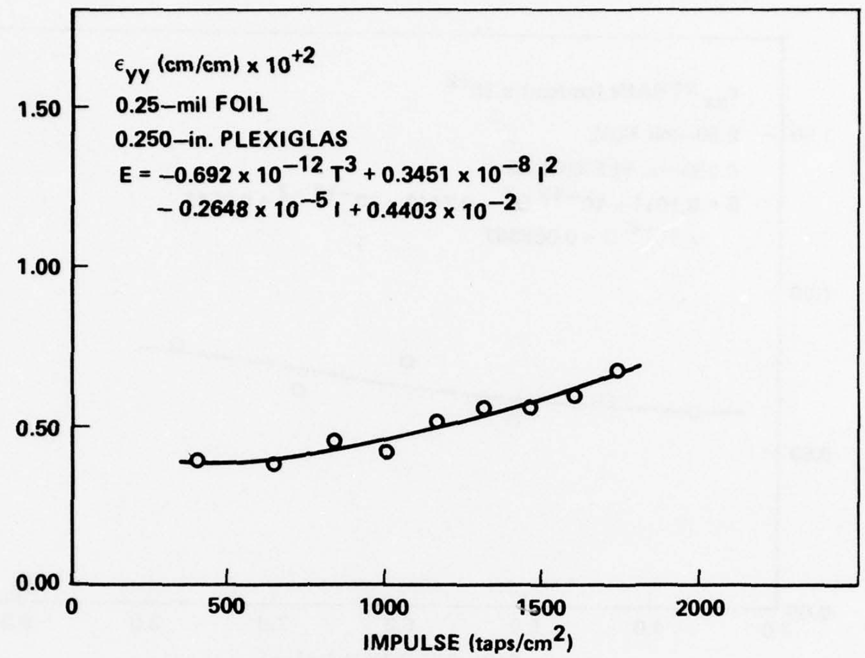

Figure 22. Plate strains as a function of foil thickness.

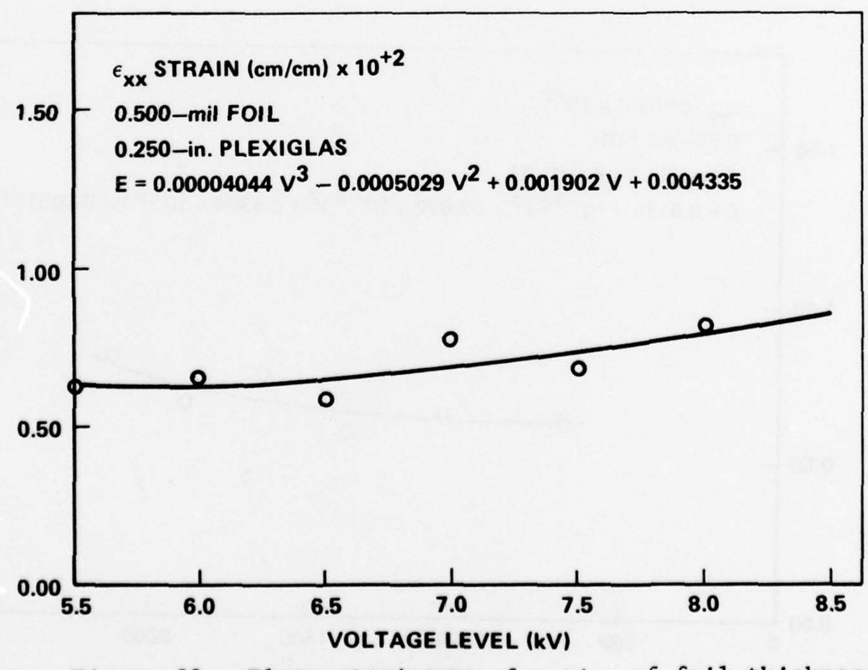

Figure 23. Plate strains as a function of foil thickness.

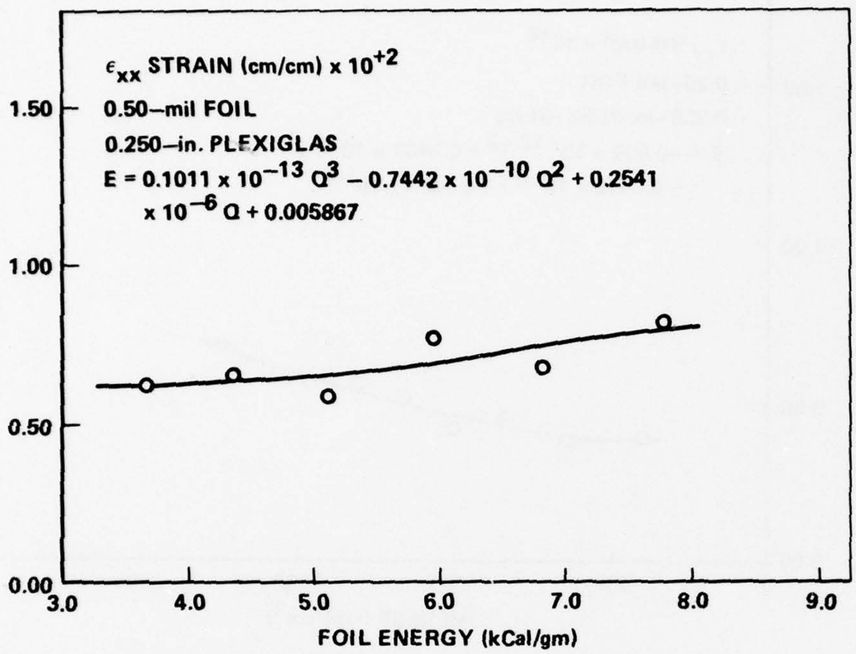

Figure 24. Plate strains as a function of foil thickness.

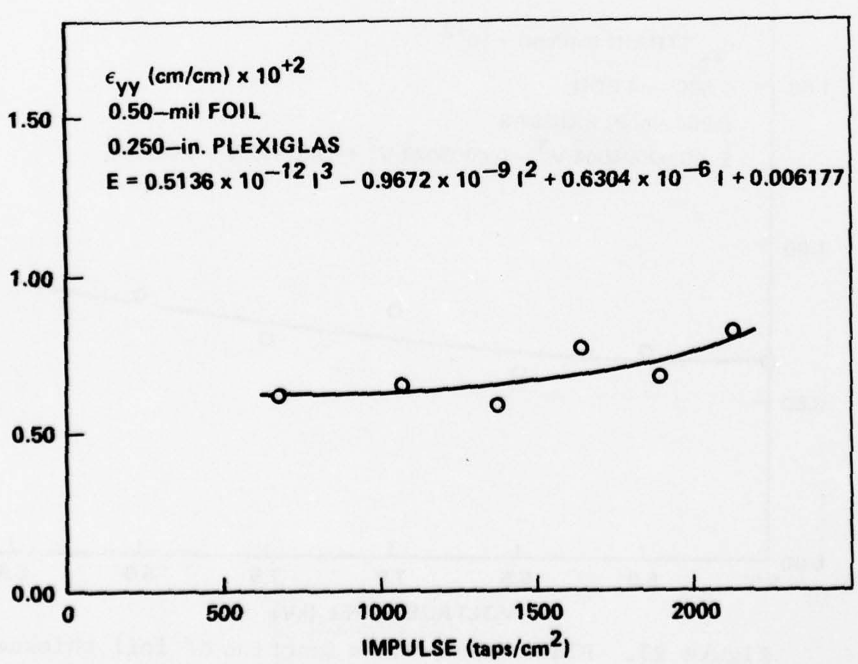

Figure 25. Plate strains as a functionof foil thickness.

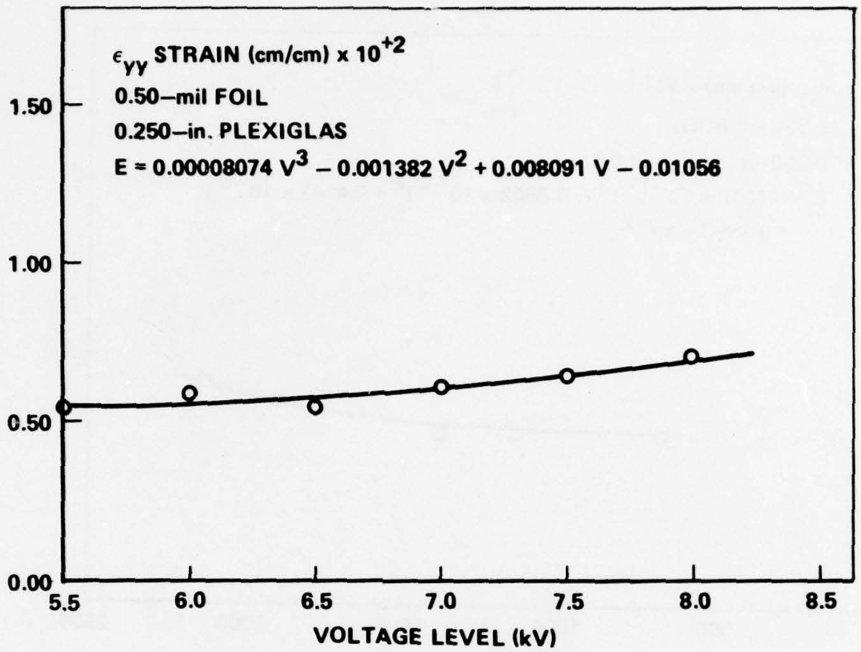

Figure 26. Plate strains as a function of foil thickness.

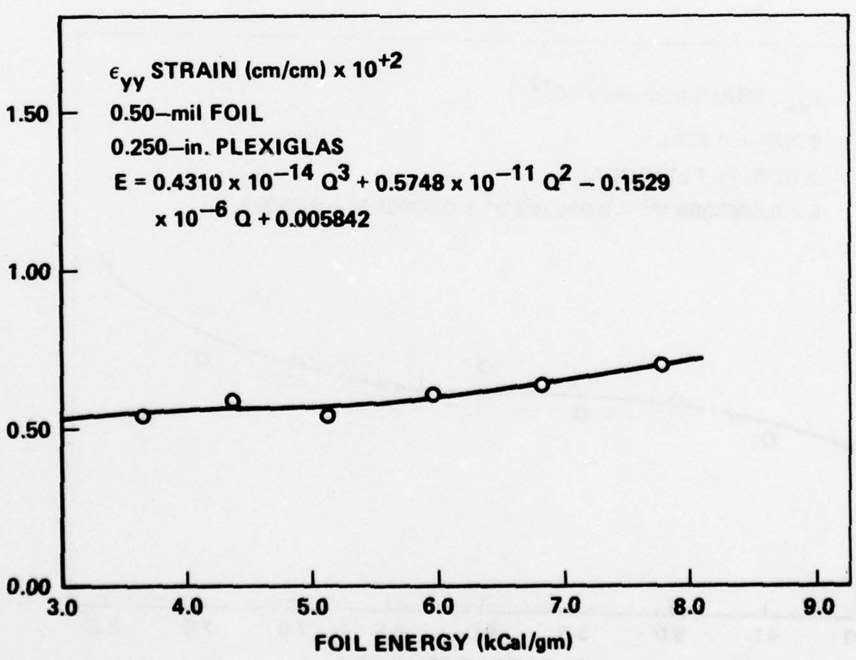

Figure 27. Plate strains as a function of foil thickness.

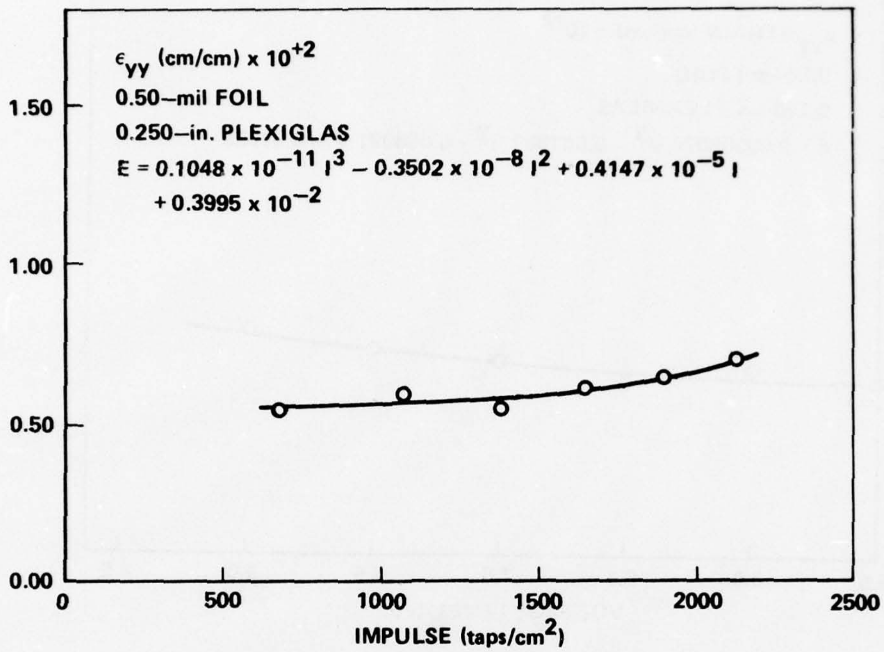

Figure 28. Plate strains as a function of foil thickness.

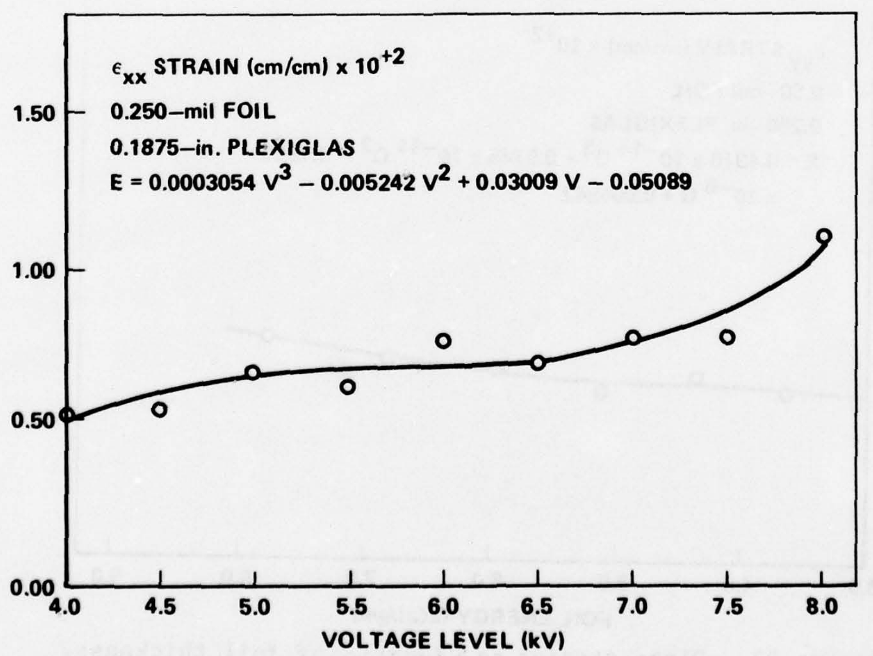

Figure 29. Plate strains as a function of foil thickness.

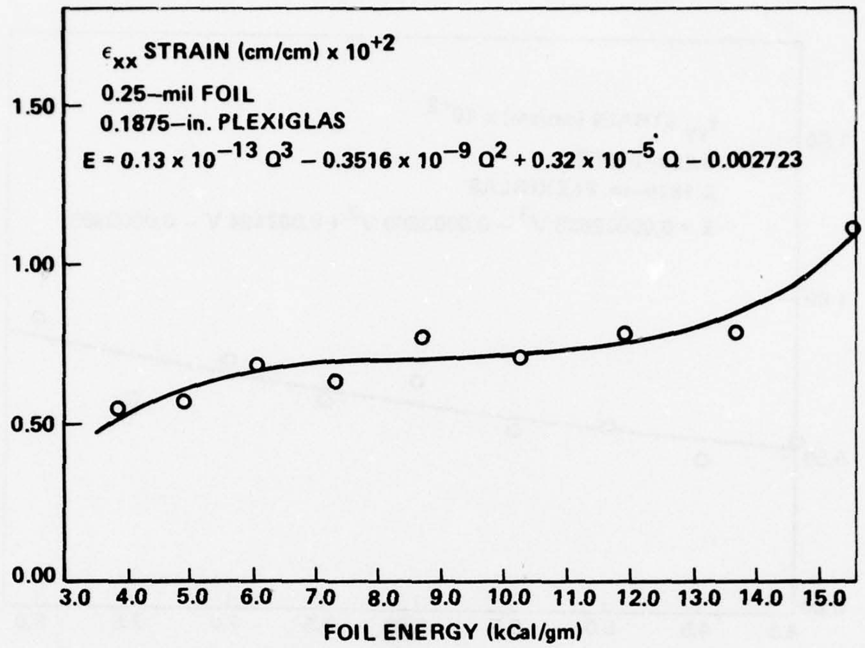

Figure 30. Plate strains as a function of foil thickness.

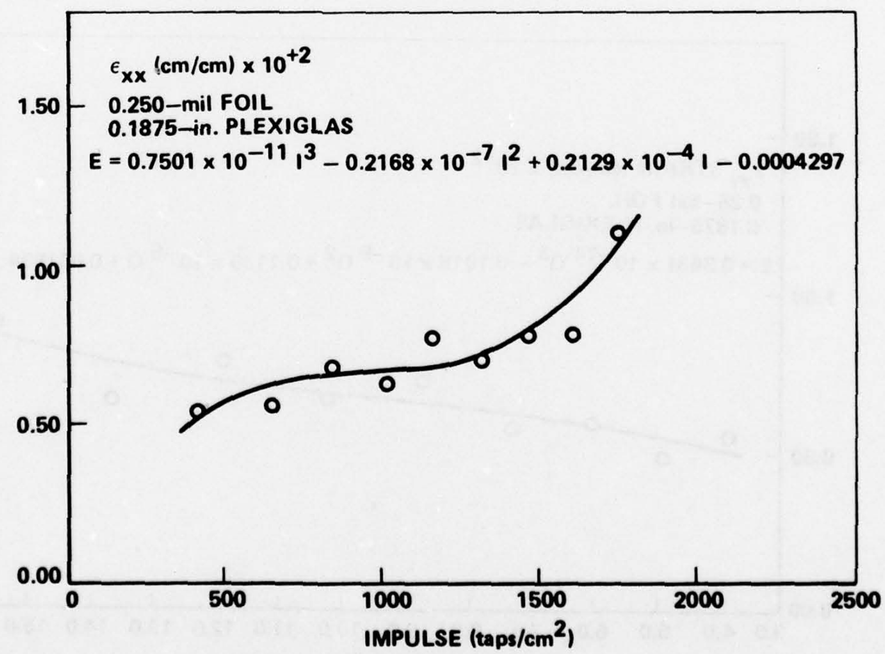

Figure 31. Plate strains as a function of foil thickness.

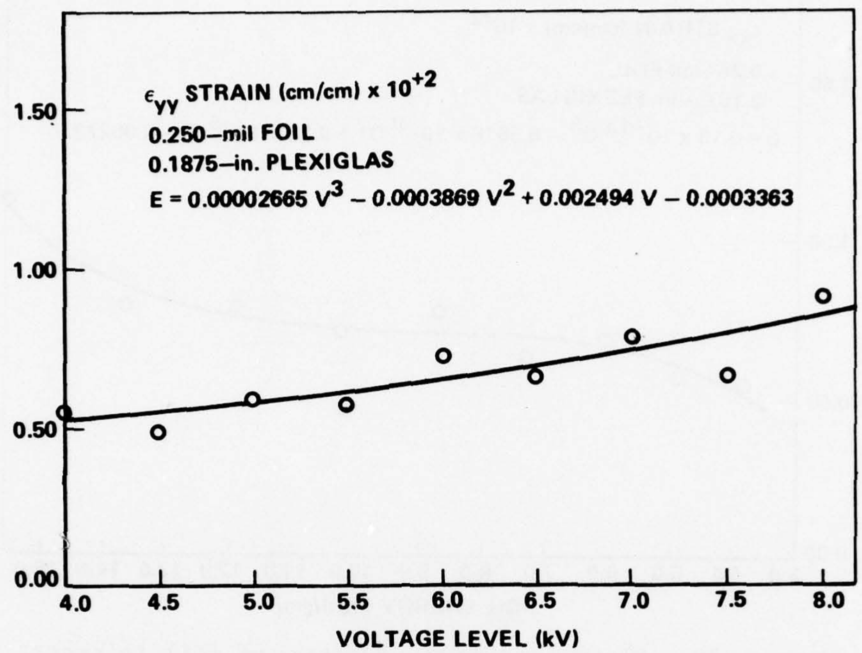

Figure 32. Plate strains as a function of foil thicknes'.

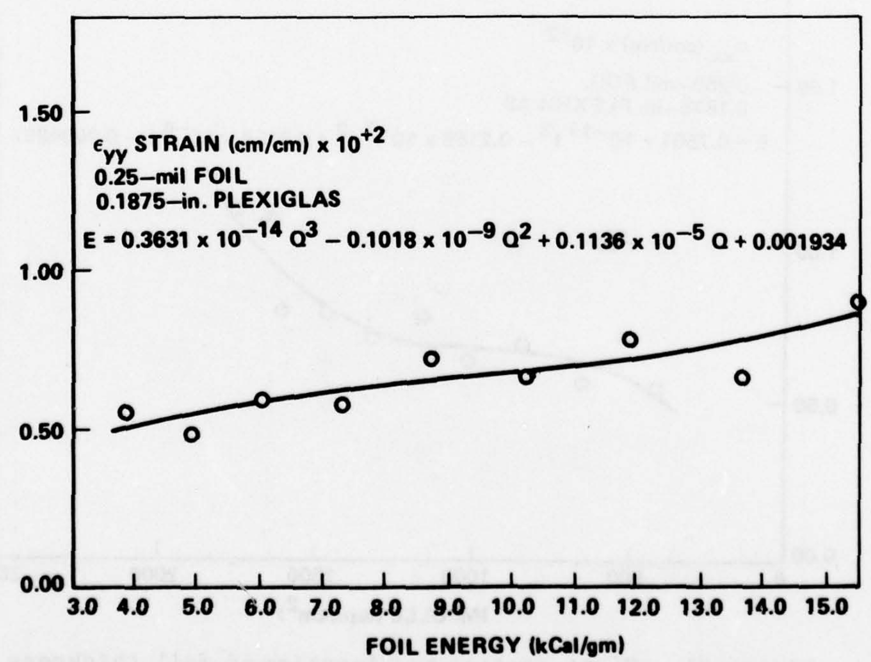

Figure 33. Plate strains as a function of foil thickness.

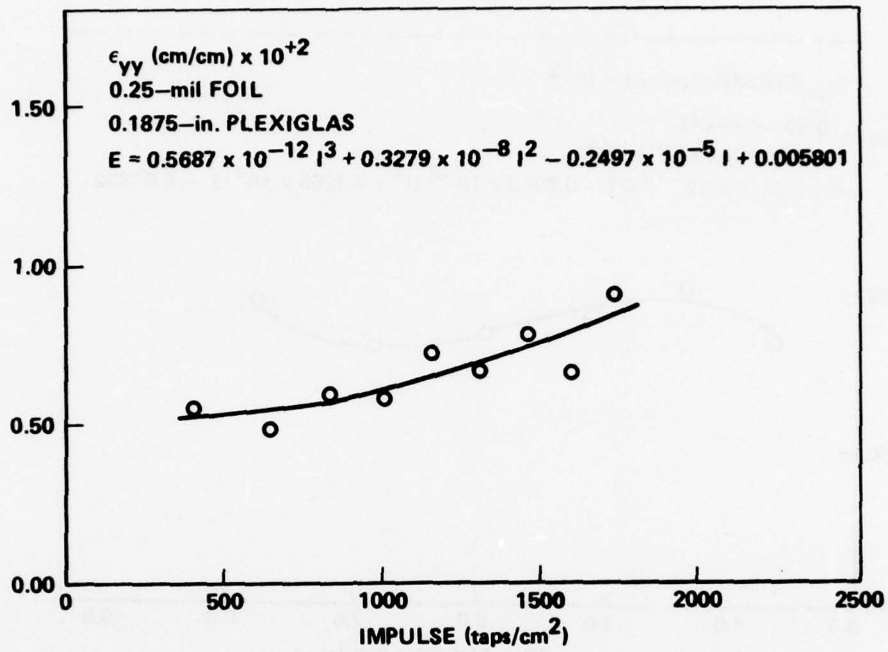

Figure 34. Plate strains as a function of foil thickness.

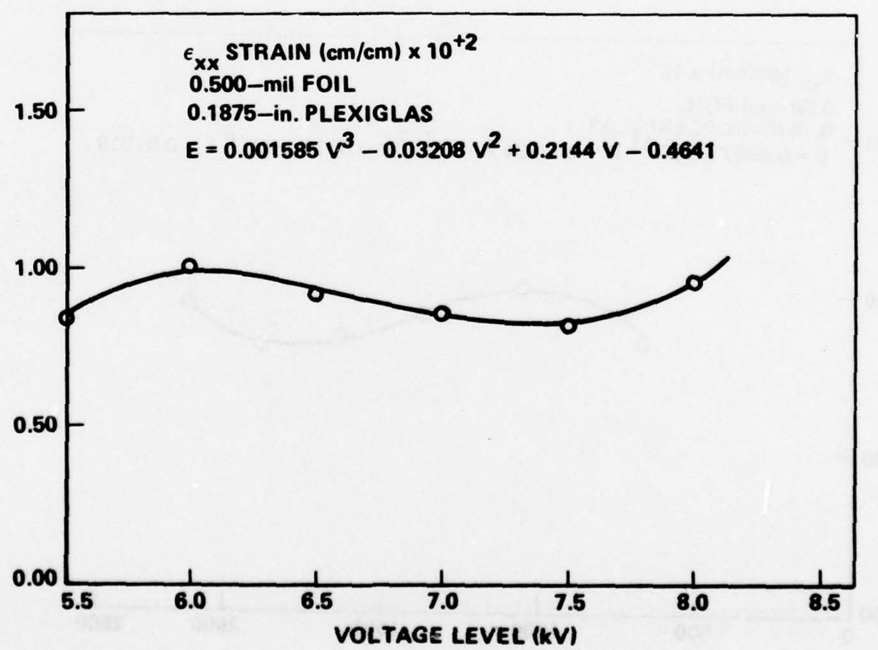

Figure 35. Plate strains as a function of foil thickness.

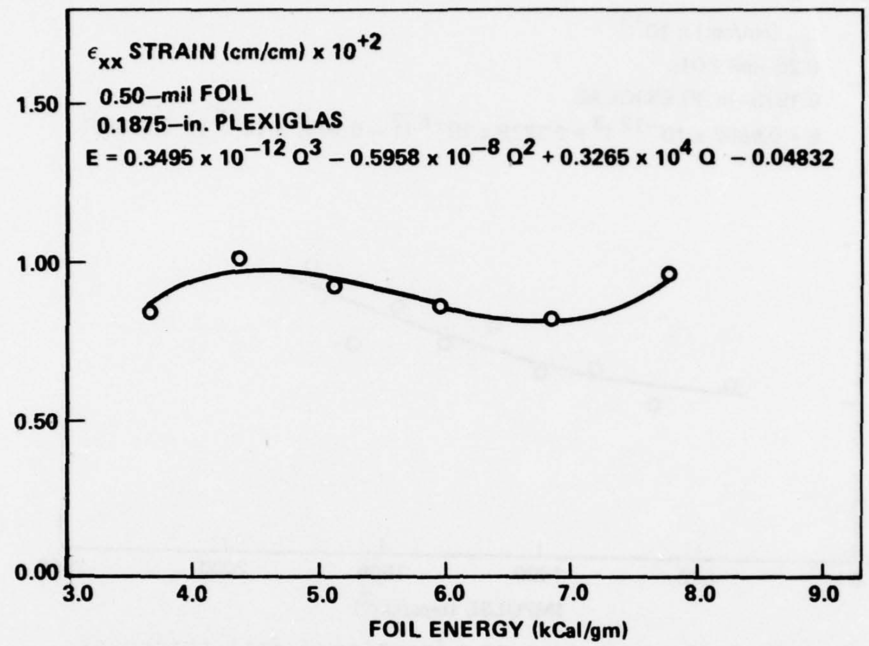

Figure 36. Plate strains as a function of foil thickness.

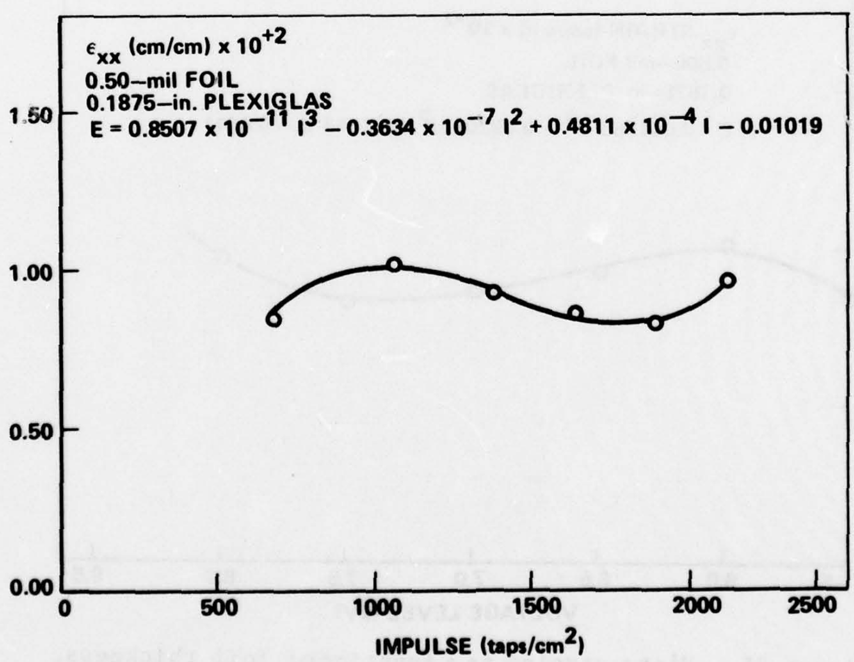

Figure 37. Plate strains as a function of foil thickness.

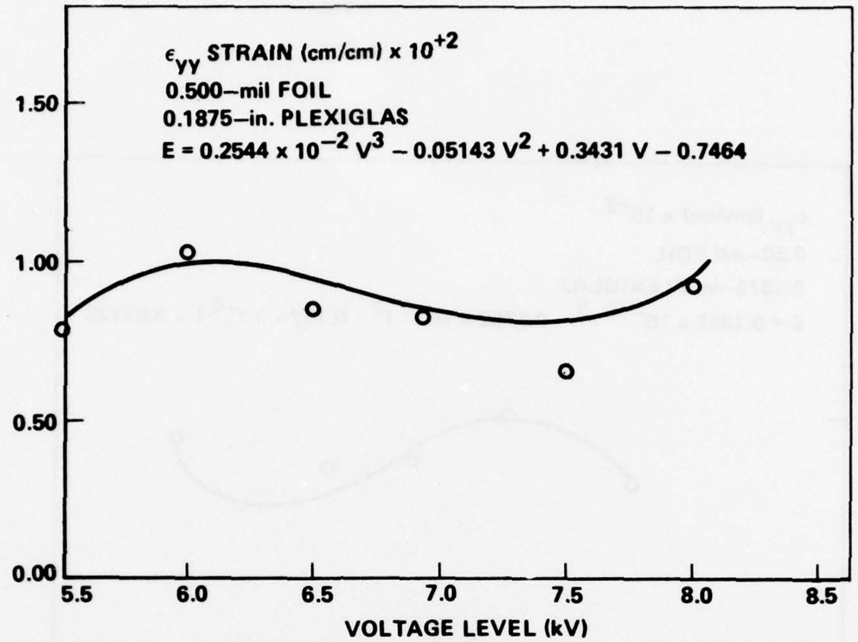

Figure 38. Plate strains as a function of foil thickness.

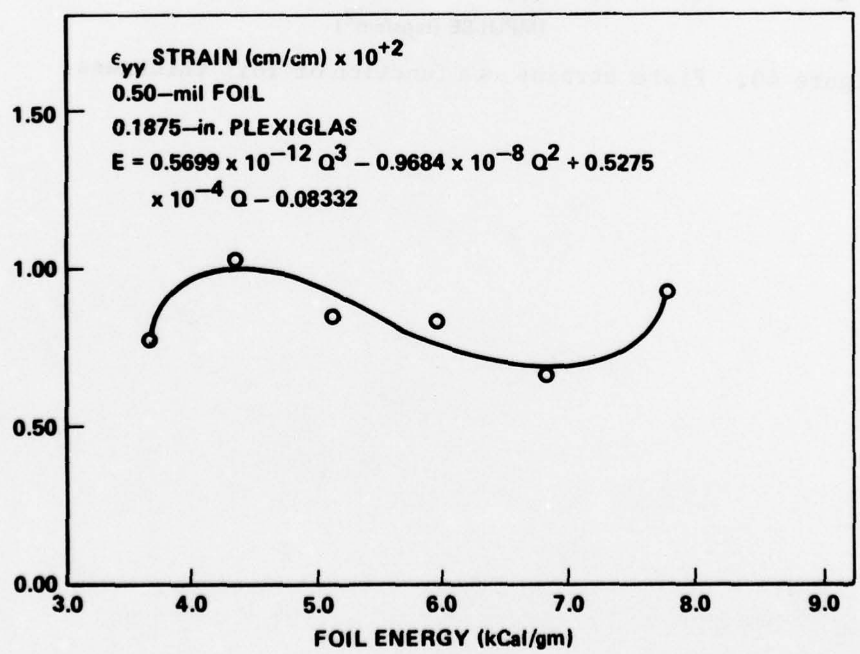

Figure 39. Plate strains as a function of foil thickness.

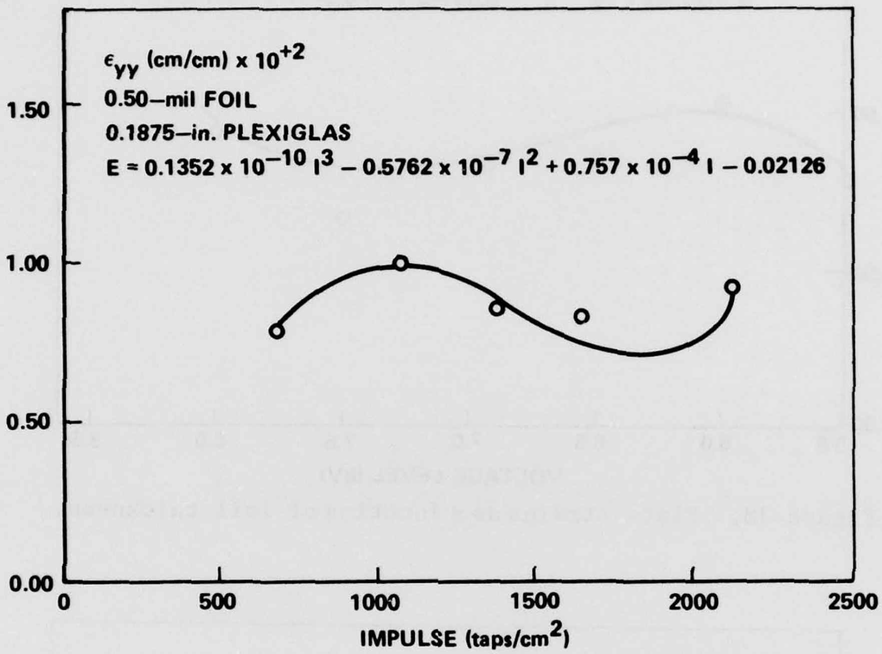

Figure 40. Plate strains as a function of foil thickness.

REFERENCES

1. Ranson, W. F., Schaeffel, J. A., Murphree, E. A., Irelan, V. G., and Mullinix, B. R., "An Experimental Assessment of Nuclear Weapons Effects of Structures," US Army Missile Command, Redstone Arsenal, Alabama, November 1975, Report No. RL-76-9.

2. Dantu P., "Me'thode nouvelle pour the de'termination des flexions dans une plaque plane," Annals des Ponts et Chausse'es, No. 1, 1940.

3. Dantu, P., "Etude experimentale des plaques par une me'thode optique" Annals des Points et chausse'es, No. 3, 1952.

4. Moore, A. D., "Soap-Film and Sandbed-Mapper Techniques," Trans. A.S.M.E Journal of Applied Mechanics, Vol. 17, No. 3, 1950 p. 291.

5. Ligtenberg, F. K., "The Moire' Method-A New Experimental Method for the Determination of Moments in Small Slab Models," Proceedings, Society for Experimental Stress Analysis, Vol. 7, No. 2, 1955.

6. Rieder, G. and Ritter, R., "Krummungsmessung an belasteten Platten nach dem Lightenbergschen Moire'-Verfahren," Forschung im Ingenieurwesen, VDI-Verlag Dusseldorf, Vol. 31, No. 2, 1965, p. 33-34.

7. Chiang, Fu-pen and Jaisingh, G., Dyanmic Moire' Methods for the Bending of Plates, Department of Mechanics Report No. 219, College of Engineering, State University of New York at Stony Brook, February 1972.

8. Theocaris, P. S., Morie' Fringes in Strain Analysis, London: Pergamon Press, 1969.

9. Durelli, A. J. and Parks, V. J., Moire' Analysis of Strain, New Jersey: Prentice-Hall Inc., 1970.

10. Cost, T. L., Griffin, J. R., and Pettey, R. H., Analysis and Design of Thermally and Mechanically Prestressed Flat Plates Subjected to Transverse Blast Loads, US Army Missile Command, Redstone Arsenal, Alabama, May 1973, Report No. RL-72-18.

11. Cost, T. L., Dynamic Response of Missile Structures to Impulsive Loads Caused by Nuclear Effects Blowoff, Athena Engineering Company, Northport, Alabama, June 1976, Report No. AEC-TR-76-01.

Appendix. COMPUTER CODES

The computer code shown on the following pages was used to reduce the plate deflection data of Tests 1 through 34. The card data input format is as follows:

Card (1)

SF,GX,GY,X,Y,Z,ZP,H,T 9F5.0 FORMAT

Card (2)

00009 This card separates the test cases.

Card (3)

IFN, X_{-2}, X_{-1}, X_0, X_{+1}, X_{+2}, Y_{-2}, Y_{-1}, Y_0, Y_{+1}, Y_{+2} I5, 10F5.0 FORMAT

•
•
•

Card (last) I5 FORMAT

00000

where

SF = Film scale factor

GX = Grid spacing in the x-direction

GY = Grid spacing in the y-direction

$\left.\begin{array}{l} X \\ Y \\ Z \end{array}\right\}$ = Location of camera lens in the specified test coordinate system

ZP = Plate to grid distance

H = Plate thickness

T = Time between film frame exposures

IFN = film frame number which identifies the time after the start of of the sublimation event in which the plate has deflected.

X_{-2}, X_{-1}, X_0, X_{+1}, X_{+2} = Location of the X-grid orders

Y_{-2}, Y_{-1}; Y_0, Y_{+1}, Y_{+2} = Location of the Y-grid orders

Following the computer code is a listing of the data used in the strain analysis.

```
      PROGRAM MAIN(INPUT,OUTPUT,TAPE5=INPUT,TAPE6=OUTPUT)
C     GRID SLOPE DEFLECTION NWER PLATE ANALYZER CODE
C     WRITTEN BY JOHN A. SCHAEFFEL, JR.
      DIMENSION X1(5),Y1(5),WX1(5),WY1(5),XS(5),YS(5)
      READ (5,1) SF,GX,GY,X,Y,Z,ZP,H,T
1     FORMAT(9F5.5)
2     READ(5,3) IFN,X1(1),X1(2),X1(3),X1(4),X1(5),
     1Y1(1),Y1(2),Y1(3),Y1(4),Y1(5)
3     FORMAT(I5,10F5.0)
      IF(IFN.EQ.0) GOTO 17
      IF(IFN.EQ.9) GOTO 15
      DO 4 I=1,5,1
      XS(I)=ABS(X1(I)-X1(3))*SF
      YS(I)=ABS(Y1(I)-Y1(3))*SF
      IF(I.LT.3) XS(I)=-XS(I)
4     IF(I.LT.3) YS(I)=-YS(I)
      DO 5 I=1,5,1
      AN=FLOAT(I)-3.
      WX1(I)=TAN(-.5*(ATAN(((AN*GX-XS(I))/ZP)+(X/Z))-ATAN((X+XS(I))/Z)))
5     WY1(I)=TAN(-.5*(ATAN(((AN*GY-YS(I))/ZP)+(Y/Z))-ATAN((Y+YS(I))/Z)))
C     CALCULATE STRAIN DATA
      X6=0.
      X5=0.
      X4=0.
      X3=0.
      X2=0.
      X13=0.
      X12=0.
      X11=0.
      Y6=0.
      Y5=0.
      Y4=0.
      Y3=0.
      Y2=0.
      Y13=0.
      Y12=0.
      Y11=0.
      DO 6 I=1,5,1
      X2=X2+XS(I)*XS(I)
      X3=X3+XS(I)*XS(I)*XS(I)
      X4=X4+XS(I)*XS(I)*XS(I)*XS(I)
      X5=X5+XS(I)*XS(I)*XS(I)*XS(I)*XS(I)
      X6=X6+XS(I)*XS(I)*XS(I)*XS(I)*XS(I)*XS(I)
      X11=X11+XS(I)*WX1(I)
      X12=X12+XS(I)*XS(I)*WX1(I)
      X13=X13+XS(I)*XS(I)*XS(I)*WX1(I)
      Y2=Y2+YS(I)*YS(I)
      Y3=Y3+YS(I)*YS(I)*YS(I)
      Y4=Y4+YS(I)*YS(I)*YS(I)*YS(I)
      Y5=Y5+YS(I)*YS(I)*YS(I)*YS(I)*YS(I)
      Y6=Y6+YS(I)*YS(I)*YS(I)*YS(I)*YS(I)*YS(I)
      Y11=Y11+YS(I)*WY1(I)
      Y12=Y12+YS(I)*YS(I)*WY1(I)
6     Y13=Y13+YS(I)*YS(I)*YS(I)*WY1(I)
      RX1=X4*X6-X5*X5
      RX2=X3*X6-X4*X5
      RX3=X3*X5-X4*X4
```

```
      RY1=Y4*Y6-Y5*Y5
      RY2=Y3*Y6-Y4*Y5
      RY3=Y3*Y5-Y4*Y4
      WX2=(RX1*X11-RX2*X12+RX3*X13)/(RX1*X2-RX2*X3+RX3*X4)
      WY2=(RY1*Y11-RY2*Y12+RY3*Y13)/(RY1*Y2-RY2*Y3+RY3*Y4)
      TL=FLOAT(IFN)*T
      EXX=(-H/2.)*WX2
      EYY=(-H/2.)*WY2
      PD=((EXX-EYY)*2./(EXX+EYY))*100.
      WRITE(6,7) IFN
7     FORMAT(14H FRAME NUMBER=,I2)
      WRITE(6,8) TL
8     FORMAT(14H ELAPSED TIME=,F10.4,1X,6H MSEC.)
      WRITE(6,9)
9     FORMAT(23H INPUT DATA X1-X5,Y1-Y5)
      WRITE(6,10) X1(1),X1(2),X1(3),X1(4),X1(5),
     1Y1(1),Y1(2),Y1(3),Y1(4),Y1(5)
10    FORMAT(10F10.4)
      WRITE(6,11)
11    FORMAT(33H INPUT DATA SF,GX,GY,X,Y,Z,ZP,H,T)
      WRITE(6,12) SF,GX,GY,X,Y,Z,ZP,H,T
12    FORMAT(9F10.4)
      WRITE(6,13)
13    FORMAT(12H OUTPUT DATA)
      WRITE(6,14) WX2,WY2,EXX,EYY,PD
14    FORMAT(5H WX2=,F10.4,1X,4HWY2=,F10.4,1X,
     14HEXX=,F10.4,1X,4HEYY=,F10.4,1X,19HPERCENT DIFFERENCE=,F10.4)
      WRITE(6,18)
18    FORMAT(28H WX1(1)-WX1(5),WY1(1)-WY1(5))
      WRITE(6,19) WX1(1),WX1(2),WX1(3),WX1(4),WX1(5),
     1WY1(1),WY1(2),WY1(3),WY1(4),WY1(5)
19    FORMAT(10F10.4)
      WRITE(6,20)
      WRITE(6,20)
20    FORMAT(2H *)
      GOTO 2
15    WRITE(6,16)
16    FORMAT(21H --------------------)
      GOTO 2
17    CONTINUE
      STOP
      END
```

TEST NO.	ELAPSED TIME	X-2	X-1	X0	X+1	X+2	Y-2	Y-1	Y0	Y+1	Y+2
					LOCATION OF GRID ORDERS (IN)						
1	.1686MS	.4745	.4893	.5045	.5180	.5333	.5273	.5120	.4971	.4825	.4665
1	.2810MS	.4645	.4822	.5000	.5174	.5353	.5350	.5182	.4998	.4820	.4646
1	.1124MS	.4593	.4905	.5000	.5202	.5394	.5415	.5208	.4990	.4774	.4575
1	.2248MS	.4654	.4928	.4997	.5166	.5339	.5326	.5169	.5004	.4842	.4672

TEST NO.	ELAPSED TIME	X-2	X-1	X0	X+1	X+2	Y-2	Y-1	Y0	Y+1	Y+2
					LOCATION OF GRID ORDERS (IN)						
2	.1686MS	.4724	.4963	.4991	.5123	.5253	.5302	.5156	.5008	.4844	.4696
2	.2810MS	.4703	.4851	.4989	.5133	.5282	.5023	.4860	.4710	.4547	.4377
2	.1124MS	.4641	.4902	.4946	.5105	.5254	.4698	.4521	.4351	.4170	.4001
2	.2248MS	.4679	.4923	.4956	.5088	.5222	.4288	.4148	.4000	.3853	.3707

TEST NO.	ELAPSED TIME	X-2	X-1	X0	X+1	X+2	Y-2	Y-1	Y0	Y+1	Y+2
					LOCATION OF GRID ORDERS (IN)						
3	.1686MS	.4724	.4863	.4992	.5129	.5264	.5288	.5150	.5003	.4874	.4730
3	.2810MS	.4649	.4821	.4995	.5157	.5322	.5081	.4908	.4733	.4562	.4391
3	.1124MS	.4730	.4869	.4993	.5129	.5252	.5304	.5151	.4996	.4851	.4700-
3	.2248MS	.4696	.4851	.4999	.5144	.5286	.5286	.5148	.5006	.4864	.4721

TEST NO.	ELAPSED TIME	X-2	X-1	X0	X+1	X+2	Y-2	Y-1	Y0	Y+1	Y+2
					LOCATION OF GRID ORDERS (IN)						
4	.1686MS	.4735	.4872	.5010	.5148	.5285	.5073	.4938	.4795	.4654	.4504
4	.2810MS	.4685	.4836	.4988	.5139	.5291	.5344	.5177	.5000	.4824	.4657
4	.1124MS	.4698	.4852	.4983	.5120	.5259	.5319	.5155	.4992	.4833	.4678
4	.2248MS	.4711	.4962	.5007	.5159	.5306	.5288	.5139	.4984	.4841	.4695

TEST NO.	ELAPSED TIME	X-2	X-1	X0	X+1	X+2	Y-2	Y-1	Y0	Y+1	Y+2
					LOCATION OF GRID ORDERS (IN)						
5	.1686MS	.4768	.4889	.4997	.5113	.5233	.5251	.5127	.4989	.4870	.4738
5	.2810MS	.4687	.4839	.4991	.5134	.5284	.5043	.4888	.4728	.4580	.4424
5	.1124MS	.4669	.4848	.4997	.5156	.5311	.5353	.5173	.4989	.4829	.4651
5	.2248MS	.4710	.4864	.4996	.5140	.5282	.5274	.5138	.4994	.4869	.4722
5	.3372MS	.4657	.4837	.5002	.5172	.5347	.5373	.5191	.5006	.4814	.4628

TEST NO.	ELAPSED TIME	X-2	X-1	X0	X+1	X+2	Y-2	Y-1	Y0	Y+1	Y+2
					LOCATION OF GRID ORDERS (IN)						
6	.1686MS	.4767	.4887	.5002	.5120	.5239	.5276	.5145	.5016	.4887	.4756
6	.2810MS	.4695	.4850	.4985	.5131	.5281	.5288	.5138	.4987	.4840	.4689
6	.1124MS	.4711	.4860	.4996	.5143	.5283	.5006	.4843	.4689	.4532	.4372
6	.2248MS	.4739	.4875	.5000	.5131	.5259	.5263	.5126	.4997	.4876	.4736
6	.3372MS	.4644	.4827	.5002	.5173	.5349	.5360	.5176	.4987	.4801	.4604

TEST NO.	ELAPSED TIME	X-2	X-1	X0	X+1	X+2	Y-2	Y-1	Y0	Y+1	Y+2
					LOCATION OF GRID ORDERS (IN)						
7	.1686MS	.4780	.4893	.4997	.5103	.5212	.5243	.5120	.4998	.4872	.4743
7	.2810MS	.4736	.4871	.4994	.5130	.5261	.5272	.5128	.4989	.4857	.4716
7	.2248MS	.4759	.4883	.5008	.5125	.5247	.5251	.5127	.4998	.4879	.4755
7	.3372MS	.4707	.4864	.5010	.5159	.5312	.5100	.4936	.4767	.4595	.4421

TEST NO.	ELAPSED TIME	X-2	X-1	X0	X+1	X+2	Y-2	Y-1	Y0	Y+1	Y+2
					LOCATION OF GRID ORDERS (IN)						
8	.1686MS	.4780	.4888	.4991	.5094	.5197	.5246	.5130	.4998	.4874	.4754
8	.2810MS	.4739	.4870	.4989	.5121	.5248	.5263	.5133	.4996	.4866	.4728
8	.2248MS	.4763	.4882	.4999	.5115	.5225	.5235	.5112	.4995	.4873	.4752
8	.3372MS	.4694	.4850	.4996	.5148	.5293	.5337	.5173	.5003	.4831	.4642

TEST NO.	ELAPSED TIME	X-2	X-1	X0	X+1	X+2	Y-2	Y-1	Y0	Y+1	Y+2
					LOCATION OF GRID ORDERS (IN)						
9	.2810MS	.5305	.5427	.5583	.5782	.6034	.4952	.4808	.4658	.4511	.4346
9	.3934MS	.4628	.4824	.5002	.5158	.5292	.5398	.5192	.4986	.4793	.4586
9	.2248MS	.4828	.4915	.4996	.5084	.5190	.4775	.4675	.4580	.4461	.4382
9	.3372MS	.4617	.4808	.4983	.5145	.5296	.5355	.5179	.4996	.4815	.4648

TEST NO.	ELAPSED TIME	X-2	X-1	X0	X+1	X+2	Y-2	Y-1	Y0	Y+1	Y+2
					LOCATION OF GRID ORDERS (IN)						
10	.1686MS	.4768	.4887	.4993	.5106	.5216	.5263	.5128	.4999	.4876	.4737
10	.2810MS	.4726	.4867	.5000	.5137	.5277	.5297	.5155	.5002	.4867	.4716
10	.3934MS	.4604	.4803	.4998	.5182	.5377	.5470	.5241	.5011	.4798	.4578
10	.1124MS	.4660	.4824	.4983	.5142	.5302	.4962	.4781	.4592	.4428	.4249
10	.2248MS	.4750	.4875	.5020	.5138	.5260	.5272	.5136	.5008	.4879	.4749
10	.3372MS	.4653	.4824	.4996	.5163	.5321	.5107	.4928	.4749	.4569	.4383

TEST NO.	ELAPSED TIME	X-2	X-1	X0	X+1	X+2	Y-2	Y-1	Y0	Y+1	Y+2
					LOCATION OF GRID ORDERS (IN)						
11	.1686MS	.4779	.4887	.4998	.5099	.5206	.4624	.4503	.4381	.4262	.4133
11	.2810MS	.4716	.4861	.5003	.5141	.5287	.5292	.5148	.5001	.4864	.4720
11	.3934MS	.4574	.4808	.5006	.5204	.5453	.5473	.5239	.5012	.4788	.4549
11	.1124MS	.4740	.4875	.4999	.5125	.5262	.5273	.5134	.4991	.4841	.4698
11	.2248MS	.4765	.4885	.5002	.5123	.5241	.5263	.5138	.5009	.4888	.4743
11	.3372MS	.4627	.4819	.5000	.5182	.5366	.5388	.5200	.5004	.4818	.4624

TEST NO.	ELAPSED TIME	X-2	X-1	X0	X+1	X+2	Y-2	Y-1	Y0	Y+1	Y+2
					LOCATION OF GRID ORDERS (IN)						
12	.1686MS	.5835	.5956	.6071	.6183	.6295	.5230	.5117	.4995	.4870	.4752
12	.2810MS	.4707	.4857	.5008	.5149	.5300	.5314	.5158	.4997	.4847	.4693
12	.1124MS	.4770	.4885	.5000	.5110	.5219	.4951	.4820	.4675	.4550	.4412
12	.2248MS	.4754	.4878	.5001	.5124	.5245	.4664	.4542	.4410	.4293	.4153

TEST NO.	ELAPSED TIME	X-2	X-1	X0	X+1	X+2	Y-2	Y-1	Y0	Y+1	Y+2
13	.1686MS	.4782	.4980	.4978	.5071	.5160	.4703	.4595	.4481	.4361	.4253
13	.2810MS	.4714	.4941	.4973	.5103	.5226	.4507	.4368	.4240	.4104	.3970
13	.1124MS	.4694	.4928	.4961	.5098	.5228	.5296	.5141	.4986	.4828	.4669
13	.2248MS	.4756	.4972	.4994	.5111	.5224	.5218	.5105	.4985	.4870	.4745

LOCATION OF GRID ORDERS (IN)

TEST NO.	ELAPSED TIME	X-2	X-1	X0	X+1	X+2	Y-2	Y-1	Y0	Y+1	Y+2
14	.1686MS	.4793	.4999	.5006	.5106	.5205	.5230	.5117	.4997	.4883	.4757
14	.2810MS	.4742	.4967	.5002	.5132	.5266	.5262	.5124	.4995	.4857	.4715
14	.3934MS	.4387	.4680	.5005	.5343	.5700	.5579	.5287	.5010	.4990	.4449
14	.1124MS	.4762	.4983	.4999	.5121	.5237	.5280	.5143	.4998	.4860	.4710
14	.2248MS	.4795	.4989	.5001	.5114	.5221	.5217	.5113	.4999	.4886	.4770
14	.3372MS	.4659	.4936	.4997	.5165	.5335	.5391	.5202	.5007	.4810	.4605

LOCATION OF GRID ORDERS (IN)

TEST NO.	ELAPSED TIME	X-2	X-1	X0	X+1	X+2	Y-2	Y-1	Y0	Y+1	Y+2
15	.1686MS	.4799	.4903	.4994	.5090	.5186	.4951	.4846	.4734	.4627	.4507
15	.2810MS	.4723	.4959	.4997	.5122	.5251	.4767	.4635	.4498	.4377	.4244
15	.1124MS	.4725	.4964	.4996	.5122	.5253	.4522	.4380	.4239	.4089	.3949
15	.2248MS	.4767	.4974	.4978	.5075	.5176	.4155	.4052	.3947	.3829	.3724

LOCATION OF GRID ORDERS (IN)

TEST NO.	ELAPSED TIME	X-2	X-1	X0	X+1	X+2	Y-2	Y-1	Y0	Y+1	Y+2
16	.1686MS	.4779	.4988	.5008	.5118	.5223	.5226	.5119	.4993	.4881	.4763
16	.2810MS	.4699	.4950	.5012	.5156	.5306	.5077	.4923	.4762	.4604	.4448
16	.1124MS	.4806	.4908	.5015	.5116	.5216	.4685	.4567	.4450	.4334	.4214
16	.2248MS	.4771	.4988	.5003	.5121	.5235	.5221	.5111	.4997	.4873	.4742
16	.3372MS	.4657	.4841	.5006	.5174	.5364	.5434	.5217	.4998	.4806	.4598

TEST NO.	ELAPSED TIME	X-2	X-1	X0	X+1	X+2	Y-2	Y-1	Y0	Y+1	Y+2
					LOCATION OF GRID ORDERS (IN)						
17	.1686MS	.4822	.4912	.5002	.5094	.5184	.4953	.4854	.4746	.4632	.4527
17	.2810MS	.4761	.4885	.4997	.5121	.5247	.4781	.4657	.4522	.4404	.4275
17	.2248MS	.4786	.4896	.5004	.5108	.5208	.5203	.5097	.4993	.4880	.4766
17	.3372MS	.4700	.4856	.5007	.5147	.5300	.5369	.5179	.5001	.4811	.4624

TEST NO.	ELAPSED TIME	X-2	X-1	X0	X+1	X+2	Y-2	Y-1	Y0	Y+1	Y+2
					LOCATION OF GRID ORDERS (IN)						
18	.1686MS	.4797	.4899	.5000	.5099	.5196	.5220	.5112	.5003	.4898	.4777
18	.2810MS	.4689	.4831	.4981	.5112	.5258	.5275	.5141	.4991	.4853	.4709
18	.3934MS	.4630	.4817	.5002	.5180	.5368	.5369	.5181	.5000	.4811	.4624
18	.1124MS	.4733	.4873	.5017	.5146	.5284	.5292	.5137	.4987	.4830	.4672
18	.2248MS	.4740	.4865	.4988	.5116	.5233	.5233	.5120	.4992	.4876	.4746
18	.3372MS	.4747	.4883	.5019	.5142	.5275	.5299	.5149	.4990	.4837	.4676

TEST NO.	ELAPSED TIME	X-2	X-1	X0	X+1	X+2	Y-2	Y-1	Y0	Y+1	Y+2
					LOCATION OF GRID ORDERS (IN)						
19	.1686MS	.4803	.4914	.5017	.5111	.5217	.5234	.5119	.5001	.4890	.4775
19	.2810MS	.4731	.4869	.5008	.5147	.5283	.5266	.5134	.4999	.4872	.4730
19	.1124MS	.4703	.4956	.5010	.5165	.5320	.5062	.4899	.4734	.4572	.4397
19	.2248MS	.4753	.4882	.5005	.5125	.5241	.5239	.5113	.4994	.4876	.4753

TEST NO.	ELAPSED TIME	X-2	X-1	X0	X+1	X+2	Y-2	Y-1	Y0	Y+1	Y+2
					LOCATION OF GRID ORDERS (IN)						
20	.1686MS	.4815	.4913	.4997	.5087	.5173	.5201	.5104	.5002	.4900	.4794
20	.2810MS	.4758	.4883	.5003	.5120	.5238	.5220	.5109	.4998	.4891	.4781
20	.3934MS	.4740	.4873	.4998	.5119	.5248	.5324	.5168	.5004	.4851	.4690
20	.2248MS	.4788	.4889	.4991	.5091	.5189	.5212	.5117	.5017	.4915	.4814
20	.3372MS	.4755	.4972	.4991	.5112	.5230	.5271	.5142	.5004	.4872	.4736

TEST NO.	ELAPSED TIME	X-2	X-1	X0	X+1	X+2	Y-2	Y-1	Y0	Y+1	Y+2
					LOCATION OF GRID ORDERS (IN)						
21	.1686MS	.4828	.4919	.5011	.5101	.5193	.4806	.4700	.4598	.4493	.4388
21	.2810MS	.4750	.4880	.5008	.5133	.5267	.4643	.4522	.4388	.4264	.4135
21	.3934MS	.4375	.4926	.5003	.5169	.5351	.4529	.4332	.4131	.3941	.3742
21	.1124MS	.4724	.4865	.4998	.5133	.5274	.5305	.5148	.4992	.4844	.4699
21	.2248MS	.4773	.4886	.5001	.5115	.5221	.5220	.5115	.4999	.4890	.4777
21	.3372MS	.4748	.4880	.5007	.5124	.5253	.5291	.5147	.5003	.4853	.4689

TEST NO.	ELAPSED TIME	X-2	X-1	X0	X+1	X+2	Y-2	Y-1	Y0	Y+1	Y+2
					LOCATION OF GRID ORDERS (IN)						
22	.1686MS	.4856	.4932	.5013	.5090	.5166	.4850	.4762	.4675	.4583	.4491
22	.2810MS	.4777	.4885	.4993	.5099	.5203	.5204	.5109	.5005	.4907	.4800
22	.3934MS	.4742	.4868	.4995	.5112	.5237	.5124	.4975	.4822	.4674	.4517
22	.1124MS	.4718	.4865	.5005	.5144	.5288	.5294	.5139	.4985	.4843	.4699
22	.2248MS	.4815	.4904	.4993	.5084	.5176	.5189	.5098	.5005	.4908	.4821
22	.3372MS	.4762	.4882	.4999	.5118	.5236	.5257	.5133	.5005	.4875	.4742

TEST NO.	ELAPSED TIME	X-2	X-1	X0	X+1	X+2	Y-2	Y-1	Y0	Y+1	Y+2
					LOCATION OF GRID ORDERS (IN)						
23	.1686MS	.4840	.4927	.5016	.5096	.5179	.5184	.5093	.5001	.4901	.4805
23	.2810MS	.4794	.4899	.5003	.5107	.5215	.5211	.5112	.5004	.4899	.4792
23	.2248MS	.4798	.4895	.4996	.5090	.5183	.5196	.5101	.5005	.4911	.4809
23	.3372MS	.4765	.4883	.5000	.5110	.5225	.5056	.4931	.4800	.4669	.4541

TEST NO.	ELAPSED TIME	X-2	X-1	X0	X+1	X+2	Y-2	Y-1	Y0	Y+1	Y+2
					LOCATION OF GRID ORDERS (IN)						
24	.1686MS	.4860	.4932	.5009	.5088	.5163	.4964	.4873	.4779	.4683	.4596
24	.2810MS	.4809	.4904	.5005	.5098	.5195	.5195	.5103	.5011	.4911	.4820
24	.3934MS	.4760	.4882	.5000	.5120	.5240	.5305	.5151	.4998	.4850	.4691
24	.2248MS	.4828	.4910	.4994	.5078	.5163	.5173	.5092	.5008	.4922	.4832
24	.3372MS	.4768	.4891	.5001	.5100	.5199	.5240	.5117	.4998	.4887	.4755

TEST NO.	ELAPSED TIME	X-2	X-1	X0	X+1	X+2	Y-2	Y-1	Y0	Y+1	Y+2
					LOCATION OF GRID ORDERS (IN)						
25	.1686MS	.4837	.4919	.4995	.5076	.5150	.5181	.5091	.4998	.4898	.4811
25	.2810MS	.4777	.4888	.4997	.5110	.5219	.5028	.4921	.4811	.4701	.4585
25	.1124MS	.4768	.4889	.5004	.5109	.5229	.5262	.5133	.5006	.4876	.4738
25	.2248MS	.4808	.4909	.5004	.5098	.5192	.4927	.4833	.4737	.4642	.4539
25	.3372MS	.4762	.4883	.5001	.5114	.5235	.5285	.5146	.5010	.4872	.4723

TEST NO.	ELAPSED TIME	X-2	X-1	X0	X+1	X+2	Y-2	Y-1	Y0	Y+1	Y+2
					LOCATION OF GRID ORDERS (IN)						
26	.1686MS	.4874	.4937	.5000	.5059	.5119	.4903	.4831	.4754	.4674	.4599
26	.2810MS	.4809	.4904	.5002	.5093	.5186	.5181	.5091	.5001	.4910	.4819
26	.2248MS	.4854	.4933	.5009	.5086	.5160	.5160	.5083	.5000	.4928	.4842
26	.3372MS	.4808	.4899	.4994	.5087	.5182	.5235	.5119	.4997	.4878	.4757

TEST NO.	ELAPSED TIME	X-2	X-1	X0	X+1	X+2	Y-2	Y-1	Y0	Y+1	Y+2
					LOCATION OF GRID ORDERS (IN)						
27	.1686MS	.4819	.4905	.4989	.5071	.5159	.5043	.4949	.4856	.4757	.4658
27	.2810MS	.4779	.4889	.5003	.5106	.5209	.5217	.5112	.5000	.4904	.4798
27	.3934MS	.4775	.4889	.4992	.5098	.5205	.5264	.5134	.5007	.4880	.4741
27	.2248MS	.4831	.4912	.4990	.5063	.5143	.4905	.4823	.4739	.4654	.4569
27	.3372MS	.4768	.4884	.5002	.5121	.5237	.4989	.4868	.4741	.4623	.4489

TEST NO.	ELAPSED TIME	X-2	X-1	X0	X+1	X+2	Y-2	Y-1	Y0	Y+1	Y+2
					LOCATION OF GRID ORDERS (IN)						
28	.1686MS	.4871	.4943	.5005	.5074	.5131	.5140	.5071	.4998	.4930	.4849
28	.2810MS	.4795	.4902	.5004	.5113	.5219	.5209	.5103	.4996	.4893	.4779
28	.3934MS	.4704	.4861	.4997	.5134	.5278	.5324	.5168	.5005	.4841	.4678
28	.1124MS	.4826	.4920	.5006	.5095	.5174	.5209	.5105	.5003	.4897	.4782
28	.2248MS	.4804	.4906	.5004	.5105	.5193	.4975	.4880	.4779	.4684	.4587
28	.3372MS	.4790	.4899	.5002	.5101	.5198	.5262	.5136	.5006	.4878	.4751

TEST NO.	ELAPSED TIME	X-2	X-1	X0	X+1	X+2	Y-2	Y-1	Y0	Y+1	Y+2
					LOCATION OF GRID ORDERS (IN)						
29	.1686MS	.4849	.4927	.4998	.5068	.5138	.5171	.5082	.4992	.4904	.4811
29	.2810MS	.4793	.4895	.4995	.5091	.5183	.5177	.5092	.4998	.4912	.4816
29	.3934MS	.4798	.4895	.4994	.5086	.5179	.5262	.5130	.4998	.4871	.4739
29	.2248MS	.4858	.4922	.4993	.5061	.5130	.4888	.4816	.4739	.4658	.4583
29	.3372MS	.4802	.4895	.4997	.5099	.5199	.5218	.5115	.4999	.4891	.4771

TEST NO.	ELAPSED TIME	X-2	X-1	X0	X+1	X+2	Y-2	Y-1	Y0	Y+1	Y+2
					LOCATION OF GRID ORDERS (IN)						
30	.1686MS	.4861	.4933	.5001	.5077	.5132	.5159	.5081	.4996	.4918	.4835
30	.2810MS	.4792	.4893	.5000	.5100	.5193	.5193	.5097	.5005	.4913	.4819
30	.3934MS	.4764	.4889	.5001	.5114	.5225	.5306	.5160	.4997	.4840	.4668
30	.1124MS	.4714	.4858	.5002	.5147	.5289	.5337	.5176	.5006	.4858	.4686
30	.2248MS	.4834	.4916	.5001	.5086	.5168	.5171	.5089	.4997	.4919	.4830
30	.3372MS	.4796	.4897	.5000	.5102	.5204	.5244	.5130	.5001	.4880	.4757

TEST NO.	ELAPSED TIME	X-2	X-1	X0	X+1	X+2	Y-2	Y-1	Y0	Y+1	Y+2
					LOCATION OF GRID ORDERS (IN)						
31	.1686MS	.4581	.4663	.4739	.4819	.4893	.4552	.4460	.4364	.4267	.4179
31	.2810MS	.4808	.4903	.5005	.5102	.5196	.5187	.5097	.5001	.4908	.4814
31	.3934MS	.4768	.4885	.5009	.5110	.5221	.5302	.5148	.5002	.4851	.4708
31	.2248MS	.4841	.4927	.5002	.5080	.5154	.5187	.5094	.4998	.4902	.4809
31	.3372MS	.4803	.4905	.5004	.5098	.5192	.5181	.5097	.4998	.4908	.4813

TEST NO.	ELAPSED TIME	X-2	X-1	X0	X+1	X+2	Y-2	Y-1	Y0	Y+1	Y+2
					LOCATION OF GRID ORDERS (IN)						
32	.1686MS	.4865	.4931	.4999	.5066	.5128	.5161	.5083	.5000	.4915	.4834
32	.2810MS	.4809	.4904	.5005	.5096	.5183	.5171	.5087	.4994	.4911	.4823
32	.3934MS	.4769	.4886	.5001	.5112	.5220	.5300	.5148	.4992	.4841	.4682
32	.2248MS	.4843	.4926	.4995	.5076	.5154	.5168	.5088	.5009	.4935	.4852
32	.3372MS	.4809	.4908	.5012	.5103	.5200	.5226	.5118	.5000	.4892	.4776

TEST NO.	ELAPSED TIME	X-2	X-1	X0	X+1	X+2	Y-2	Y-1	Y0	Y+1	Y+2
					LOCATION OF GRID ORDERS (IN)						
33	.1686MS	.4881	.4996	.5009	.5074	.5136	.4876	.4807	.4728	.4655	.4580
33	.2810MS	.4793	.4898	.5003	.5107	.5206	.5210	.5107	.5000	.4895	.4782
33	.1124MS	.4842	.4917	.4997	.5072	.5140	.5180	.5089	.4999	.4911	.4807
33	.2248MS	.4804	.4905	.4998	.5085	.5174	.5167	.5081	.4987	.4899	.4806
33	.3372MS	.4789	.4896	.5002	.5108	.5205	.5295	.5151	.5000	.4863	.4722

TEST NO.	ELAPSED TIME	X-2	X-1	X0	X+1	X+2	Y-2	Y-1	Y0	Y+1	Y+2
					LOCATION OF GRID ORDERS (IN)						
34	.1686MS	.4858	.4928	.4995	.5057	.5123	.5148	.5072	.4986	.4913	.4831
34	.2810MS	.4798	.4897	.4998	.5092	.5190	.5189	.5098	.5005	.4917	.4823
34	.1124MS	.4739	.4869	.4996	.5118	.5255	.5144	.4986	.4833	.4685	.4543
34	.2248MS	.4829	.4916	.5000	.5082	.5165	.5168	.5087	.5000	.4919	.4826
34	.3372MS	.4779	.4889	.5000	.5105	.5212	.5264	.5133	.5001	.4879	.4749

DISTRIBUTION

	No. of Copies
Defense Documentation Center Cameron Station Alexandria, Virginia 22314	12
Commander US Army Materiel Development and Readiness Command	
Attn: DRCRD	1
DRCDL	1
5001 Eisenhower Avenue Alexandria, Virginia 22333	
Office of Naval Research	
Attn: Mr. A. M. Diness, ONR 471	1
800 North Quincy Street Arlington, Virginia 22217	
Superior Technical Services, Inc.	
Attn: T. Ward	1
4308 Governors Drive Huntsville, Alabama 35805	
DRSMI-LP, Mr. Voigt	1
DRDMI-T, Dr. Kobler	1
-TER, Mr. R. Russell	1
-TG	1
-TL, Mr. Lewis	2
-TLA, Mr. Pettey	12
-TLA, Dr. B. Mullinix	31
-EA, Mr. Greene	5
Mr. Matthews	1
-TBD	3
-TI (Record Set)	1
(Reference Copy)	1